

Special Issue of the Asian Journal of Control
“Control Biology—Emerging Field of Life Science
that Connects Biology and Control”
Sensory Motor Instability and Central Pattern
Generator in Spinal Oscillations *

Edmond Jonckheere,[†] Poonsuk Lohsoonthorn & Vikram Mahajan
Electrical Engineering Dept. & Biomedical Engineering Dept.
University of Southern California
Los Angeles, CA

Abstract

An electrophysiological phenomenon running along the spine, referred to as Network Spinal Analysis (NSA) wave, is analyzed from the point of view that it is created by a sensory-motor loop instability, itself settling in a Central Pattern Generator (CPG). The major investigative tool is surface electromyographic (sEMG) signal analysis at various points along the paraspinal muscles. The sEMG signals appear to consist of a great many “bursts,” hinting at a global synchronization of the firing of the spinal neurons. Statistical correlation among the various signals recorded at various points along the spine is used to identify the propagation delay of the bursts from one point to another and hence to establish the traveling wave phenomenon, itself settling in a stationary wave phenomenon on a specific subband of the Daubechies wavelet decomposition of the signals. As such, the spine is viewed as a propagation medium, with the sensory-motor loops at the cervical and sacral areas providing boundary conditions on which the wave reflects. As a therapeutic application, it is shown that a quadriplegic patient with a cervical spinal cord injury not only was able to experience the wave, but did recover some partial sensory and motor functions. The partial motor recovery from the spinal cord injury was assessed by the correlation between the sEMG signals on both sides of the injury. The same quadriplegic patient analysis reveals that the nervous pathways need not go via the brain, are confined within the spinal cord, hence indicating the presence of a Central Pattern Generator.

*The research, which involves human subjects, was approved by the Institutional Review Board (IRB) of the University of Southern California and was supported by the Association for Network Care Research Corporation.

[†]Corresponding author, 3740 McClintock Avenue, Room EEB 306, Los Angeles, CA 90089-2563, jonckhee@usc.edu, tel: (213) 740-4457, fax: (213) 821 1109.

key words: surface Electromyography (sEMG), correlation, wavelets, Central Pattern Generator (CPG), sensory-motor instability, dural mechanoreceptors, regeneration in the Central Nervous System (CNS).

1 Introduction

1.1 neurosurgical background

In a book [2] that has captured the attention of spine health professionals, the Scandinavian neurosurgeon Alf Breig introduced the concept of *Adverse Mechanical Tensions in the Central Nervous System*. The tenet of this theory is the fact that, at the cranial level, the dura mater of the spinal cord is mechanically attached to the circumference of the foramen magnum. The dentate ligament in the subaracnoid space transmits the tension to the pia matter and hence to the cord. Anatomically, the dentate ligament acts as a device that hangs the cord to the foramen magnum so that excessive load on the midbrain, the pons, and the medulla be avoided. In addition to the attachment of the dura to the ring of the atlas, there is also evidence [27] of direct attachments of the dura to the osseous structures of the vertebra at the C2-C6 levels, although it seems that there is considerable variation among individuals.

At the sacral level, the distal end of the cord is attached to the coccyx via the *filum terminale*. Anatomically, the *filum terminale* acts like a rubber band that gently stretches the spinal cord and allows the cord to sustain considerable length variation under flexion and extension.

While the spine is normally stretched, mechanical tensions in the cord become “adverse” in Breig’s sense when the movement of the cord is restricted by injury, space-occupying lesions, or scar tissue (e.g, tethered cord syndrome). Other sources of pathological tensions include postural problems. These adverse tensions themselves decrease nerve conductivity [3], hence impair nerve activity. Pathological tensions also induce hyperstimulation of the proprioceptive fibers afferent to the spine, resulting in impaired functionality of the spine at the attachment level and other effects at other parts of the nervous system. It has been argued by Breig that some diseases (including multiple sclerosis [2, p. 177]) have this neuro-biomechanical origin and that relieve of these adverse tensions could alleviate symptoms [3].

1.2 sensory-motor instability, central pattern generator, and spinal oscillations

The present paper deals with the fact that the dural attachments create paths from the mechanical movement of the spine to the Central Nervous System (CNS). In the motor reflex loop, the degree of stretch of the paraspinal muscles is recorded by the neuromuscular spindles and transmitted by afferent fibers to the motor neurons in the spine, back to the muscles via the efferent fibers [22, p. 41, 139]. However, the dural attachment creates an extra path from the

paraspinal muscles *directly* to the spinal neurons, hence closing the loop, as shown in Figures 20, 21. The existence of this feedback loop has been demonstrated by the spinal oscillators, which can be elicited by a technique referred to as *Network Spinal AnalysisTM (NSA) care*. In this technique, the practitioner locates the Spinal GatewayTM area, which is on the skin overlying or in the vicinity of the dural-vertebral attachments, based on his (her) professional assessment of the status of the active, passive, and neural subsystems supporting the normal function of the nervous system [20], and sensitizes the areas to the point where a slight pressure at the spinal gateway area elicits an oscillation that takes, initially, the form of a slight muscular movement or localized twitch in the neck area.

Likewise, an oscillation can also be elicited at the sacral level, where the feedback mechanism is provided by the attachment of the *filum terminale*, the distal end of the spine, to the coccyx.

The cervical, sacral oscillators create waves propagating downward, upward, respectively, along the spine, until they take the external appearance of a spontaneous rocking motion of the spine, referred to as *NSA wave*. Kinematically, the NSA wave looks like the swimming of a dolphin. The NSA wave is involuntarily controlled, but can be voluntarily stopped.

As the research subject volunteers to be under NSA care, (s)he progresses through several *levels of care*: Level 1, Level 2, Level 3. Roughly speaking, the *level of care* is the number of spinal oscillators engaged. At the early stage, the practitioner locates the dural-vertebral attachments in the cervical area, the cervical oscillator becomes engaged, and the subject is at Level 1. Later during entrainment, the sacral oscillator becomes engaged (Level 2), and, finally, the chess-thoracic oscillator becomes active (Level 3).

The NSA wave at higher levels of care produces a rather intensive exercise for the spine and the back musculature, not reproducible by any other physiotherapeutical means. It has also been claimed to relieve *adverse mechanical tensions* in the cord. This involuntary physical activity is of the same kind as the repetitive activity that has shown therapeutic benefits for a five years post injury quadriplegic patient [18]. In fact, as the study of Section 5 demonstrates, another quadriplegic patient with a similar injury recovered some sensory and motor functions after NSA care.

1.3 surface electromyographic signal analysis

The cervical and sacral oscillations are studied in a most convenient, noninvasive manner by surface electromyographic signal analysis. These signals show considerable “bursting” activity [17, 8, 14], which makes their modeling non-trivial.

To positively confirm the wave phenomenon, an array of sEMG sensors [11] are put along the paraspinal muscles, and the signal X at some point is statistically correlated with the time-shifted version of another signal Y recorded at another point along the spine. In the first, traveling wave, analysis (Section 3.1), the mutual information between a signal at one point and the time-shifted signal

at another point is investigated. The delay achieving maximum mutual information is the time it takes for the wave to travel from one point of sEMG recording to the other. This has proved consistent with accepted values of action potential propagation. In the second, stationary wave, analysis (Section 3.2), the correlation among the sEMG phenomena along the spine is shown to provide a phase shift and is hence used to construct the “mode shape,” typical of a stationary wave.

The mathematical model that is developed here consist in treating the spine as a propagation medium, in which the cervical and sacral feedbacks provide boundary conditions, themselves creating traveling wave setting in a stationary wave.

1.4 outline of paper

The paper starts with a temporal signal analysis (Sec. 2), specialized to the cervical area, since it appears to be the origin of the wave phenomenon. Then the spatio-temporal analysis follows (Sec. 3), with the objective of understanding the propagation of the wave phenomenon along the spine. The following two sections (Sec. 4, 5) analyze, from the aforementioned viewpoint, the signals recorded on a normal, baseline research subject and those recorded on a quadriplegic patient. The objective of the baseline analysis is to positively confirm the wave phenomenon. The objective of the analysis on a quadriplegic subject is two-fold: First, it is observed that the quadriplegic patient can exhibit the NSA wave. The latter is important, since it provides the clue that the nervous pathways need not go via the brain, which points to a central pattern generator [19]. Second, it is shown that, like the Christopher Reeve case [18], the NSA wave provides a repetitive motion that appears to produce some regeneration in the Central Nervous System. Finally, in the last section (Sec. 6), we propose a thought provoking question: Whether the NSA wave is a sensory-motor instability [13] or a Central Pattern Generator [19].

2 temporal signal analysis

By *temporal* analysis of the signal, we mean the analysis of *one single* sEMG signal at *one single* point along the spine, independently of the other signals at other points. One substantial difficulty is that the sEMG signals appear to be consisting of “bursts” of accrued sEMG activity on top of a “background” signal. There are several aspects to such signals.

2.1 Switching ARIMA modeling of bursty cervical signal

The cervical sEMG signal appears to the naked eye as a series of bursts on top of a “background” signal. As the research subject progresses through higher and higher levels of care, the sEMG signals become more and more bursty. This calls for a dynamical model switching between two modes and a discrimination

criterion. The discrimination criterion is based on the observation that the background signal is, in general, less stationary than the burst signal, in the sense that the absolute sum of the sample autocorrelation of the incremental signal is larger for the background than for the burst [17]. Because of the lack of stationarity, both models have a root of unity. Hence the dynamics switches between two ARIMA models, with the switching logic based on a threshold of the sample autocorrelation sequence [17].

There is a surprising resemblance between the bursts of the sEMG signal as reported in [17] and the bursts in the electrophysiological activity recorded by microelectrodes along the axons of cultured spinal cells [8]. Equally surprising is the resemblance between the accrued bursting under advancement in the level of NSA care the accrued bursting under neurotransmitter in the cell culture. From these observations, it is fair to conjecture that the sEMG bursts in NSA care result from the large scale synchronization of the firing of the neurons [24].

2.2 Nonlinear ACE analysis

Since the residual of the ARIMA modeling does not appear Gaussian [17, Sec. 5], it is tempting to remedy this deficiency by going to such nonlinear modeling as the Alternating Conditional Expectation (ACE) [4], itself closely related to the nonlinear canonical correlation [15]. ACE produces a nonlinear model of the form

$$X(k+1) = \sum_{i=0}^{L-1} \phi_i(X(k-i))$$

from an experimental time series $\{X(k)\}$.

On a Level 2 subject, the ACE modeling of a typical burst revealed that there are about 5 significant functions [1], all of them fairly linear around the origin and then saturating. On other subjects [17, Sec. 5], the ACE modeling of both the burst and the background signal revealed an even lower order model.

On a general tone, it was found, a bit surprisingly, that the switching ARIMA strategy outperforms the switching ACE strategy in its ability to predict the data outside the training set. Thus the accrued complexity of ACE does not seem to be warranted.

2.3 difference among cervical, thoracic, lumbar, and sacral signals

There are marked difference between, on the one hand, the cervical and sacral signals and, on the other hand, the thoracic and lumbar signals. The former have higher model orders than the latter. This can be justified by the fact that precisely at the cervical and sacral levels does the complex feedback mechanism of the dural-vertebral attachments occur. This is further confirmed by the canonical correlation coefficient sequence of the signals of a Level 2 subject shown in Figure 1, revealing a much higher model order for the cervical and thoracic signals than for the lumbar and sacral signals.

2.4 discrimination among levels of care

As the care progresses through the various levels, the NSA wave itself both visually and mathematically [17, 12] undergoes significant changes. Among other factors affecting the mathematical properties of the wave is the position of the research subject during the entrainment (supine, prone, sitting).

The first change is that the Akaike mutual information between the past and the future of the signals increases with the level of care [9].

From the modeling point of view, the signal models appear quite level specific and also position specific. In fact, for a research subject entrained from early Level 1 to advanced Level 3, a set of 12 baseline ARIMA models was developed and during entrainment the best fitting model was plotted versus the entrainment time, resulting in a staircase diagram, itself revealing the level and position dependency of the model [12, 11].

3 Spatio-temporal multi-scale signals analysis

By *spatio-temporal analysis*, we mean the analysis of the sEMG signals in both the space variable (the position along the spine) and the usual time variable. The purpose of it is to positively establish the traveling wave phenomenon between the neck and the sacrum during NSA care. The *multi-scale* aspect of the analysis is the fact that only on a subband of the Daubechies wavelet decomposition of the various signals does the wave appears stationary.

The first analysis (Section 3.1) is the *canonical correlation* of the past sEMG process at some point along the spine and the time-shifted future sEMG process at another point. Quantitatively, the analysis proceeds via the singular values to the *mutual information* between the past of the process at one point and the future of the time-shifted process at the other point. The rationale is quite simple: Should there be a need of a time-shift to observe a maximum mutual information, then it can be argued that there is a wave traveling *from* the first point *to* the second point. In fact, the first point can be identified as the “cause” while the second point is identified as the “effect.”

The second analysis (Section 3.2) is computationally simplified by treating the sEMG phenomena at the 4 points along the spine as a collection of 4 random variables. It relies on the *correlation* analysis of one random variable with the time-shifted version of the random variable at another point. The advantage of this new method is that the correlation provides the cosine of the phase angle between the signal at one point and the time-shifted version of the signal at the other point. As such, a consistent phase pattern with “zero crossing nodes” would reveal a *stationary* wave phenomenon and would in fact give some clues about the mode shape.

The simplified correlation analysis is itself done on both the raw signal (Sec. 3.2.1) and a selected subband of the wavelet decomposition of the signal (Sec. 3.2.2). The latter indeed reveals the stationary wave phenomenon more clearly.

3.1 Canonical correlation among time-shifted signals at various points

The time-shifted linear canonical correlation analysis proceeds as follows: Let T_s be the time-shift and L be the ‘‘lag,’’ that is, the order of the model that would result from this analysis. Let $X(k)$ and $Y(k)$ be the sEMG signals at two points along the spine. Then the past observation of the (zero-mean) process X at time k is

$$X_-(k) = (X(k), \dots, X(k-L+1))^T$$

and the future observation of the (zero-mean) process Y at time k is

$$Y_+(k) = (Y(k+1), \dots, Y(k+L))^T$$

The canonical correlation matrix between the (zero-mean) processes $X_-(k)$ and $Y_+(k+T_s)$ is

$$\Gamma(T_s) =$$

$$(EX_-(k)X_-^T(k))^{-1/2} (EX_-(k)Y_+^T(k+T_s)) (EY_+(k+T_s)Y_+^T(k+T_s))^{-1/2}$$

where $Q^{-1/2}$ denotes the inverse of the Cholesky factor or symmetric square root of $Q = Q^T > 0$. This matrix can be singular value decomposed as

$$\Gamma(T_s) = U(T_s) \Sigma(T_s) V(T_s)$$

where $U(T_s)$ and $V(T_s)$ are orthonormal matrices and $\Sigma(T_s)$ is a diagonal matrix of $\sigma_i \in [0, 1], i = 1, \dots, L$, called time-shifted *canonical correlation coefficients*.

This approach is statistically implemented as follows: Define the crosscorrelation between the past observation of the process X and the future observation of the process Y , time shifted by T_s , to be the $L \times L$ matrix

$$C_{X_-Y_+}(T_s) = \frac{1}{K-2L+1} \sum_{k=L}^{K-L-T_s} X_-(k)^T Y_+(k+T_s)$$

Define the autocorrelation of past observation as

$$C_{X_-X_-} = \frac{1}{K-L+1} \sum_{k=L}^K X_-(k)^T X_-(k)$$

and the autocorrelation of the future observation as

$$C_{Y_+Y_+} = \frac{1}{K-L+1} \sum_{k=0}^{K-L} Y_+(k)^T Y_+(k)$$

Define the Cholesky decompositions of $C_{X_-X_-}$ and $C_{Y_+Y_+}$ as

$$\begin{aligned} C_{X_-X_-} &= T_{X_-}^T T_{X_-} \\ C_{Y_+Y_+} &= T_{Y_+}^T T_{Y_+} \end{aligned}$$

where T_{X_-} and T_{Y_+} are lower triangular matrices. The canonical correlation matrix with time-shift T_s is estimated as

$$C(T_s) = T_{X_-}^{-T} C_{X_- Y_+}(T_s) T_{Y_+}^{-T}$$

The singular values of the above matrix are collected in decreasing order along the diagonal of another matrix denoted as $S(T_s)$. The predictability of the future of the time-shifted sequence Y given the past of the sequence X is characterized by the past/future mutual information

$$I_{XY}(T_s) = -\frac{1}{2} \log \det \left(I - S(T_s)^2 \right)$$

where I is the identity $L \times L$ matrix. Define the optimal time shift T_s^* as follows:

$$T_s^* = \arg \max_{0 < T_s \leq K} I_{XY}(T_s)$$

Existence of some mutual information between $X_-(k)$ and $Y_+(k + T_s)$ indicates existence of a regression relation that could take either form:

$$\begin{aligned} Y_+(k + T_s) &= AX_-(k) + b \\ X_-(k) &= A'Y_+(k + T_s) + b' \end{aligned}$$

The first one is usually referred to as construction of the *state over the past* while the second one is construction of the *state over the future*. Which regression should be preferred depends on the behavior of the mutual information I_{XY} with T_s . On the raw signal, it was found that $T_s^* > 0$, so that this parameter can be interpreted as the propagation delay of some wave along the spine traveling from the point of observation of X to the point of observation of Y . In other words, X is the cause and Y is the effect, Y is the delayed response to X , and the first regression should be preferred. Clearly, this analysis would yield a dynamical model of Y driven by the “excitation” X .

We conjecture that this situation would typically happen if X is observed at the point along the spine where the practitioner applies pressure and Y is observed at another point along the spine.

Remark: The chief difference between the above-described analysis and the previous one reported in [1] is that, in the previous one, we did the canonical correlation analysis of the past and the future of *the same signal at the same point along the spine*, whereas, here, we do the canonical correlation analysis of the past of *one signal* and the *time-shifted* future of *another signal at another point along the spine*. The previous analysis would yield an innovation model of the process at a single point, while the present one would yield a model of Y driven by X .

Remark: The linear canonical correlation analysis is, strictly speaking, relevant only to the case of Gaussian signals, which is a problematic assumption here¹. The reason why we feel the linear canonical correlation analysis is adequate is

¹This assumption could be removed by bootstrapping.

that we observed that the nonlinear canonical correlation analysis produces only a moderate increase of the canonical correlation coefficients compared with the linear case [1]. Also the Alternating Conditional Expectation (ACE) modeling of the sEMG signal as $X(k+1) = \sum_{i=0}^{L-1} \phi_i(X(k-i))$ revealed regression functions ϕ_i fairly linear around 0 and then saturating [1].

3.2 Correlation among time-shifted phenomena at various points

A somewhat simplified approach is to compute the *scalar* correlation coefficient between the *random variables* $X(k), Y(k+T_s)$, rather than computing the canonical correlation *matrix* between the random vectors $X_-(k), Y_+(k+T_s)$. The scalar correlation coefficient [5, p. 74] between the random variables $X(k)$ and $Y(k+T_s)$ is defined as

$$\rho(T_s) = \frac{E((X(k) - EX(k))(Y(k+T_s) - EY(k+T_s)))}{\sqrt{E(X(k) - EX(k))^2} \sqrt{E(Y(k+T_s) - EY(k+T_s))^2}}$$

This approach is statistically implemented as follows [5, Chap. 12]:

$$r(T_s) = \frac{\sum_{k=1}^{K-T_s} (X(k) - \bar{X}(T_s)) (Y(k+T_s) - \bar{Y}(T_s))}{\sqrt{\sum_{k=1}^{K-T_s} (X(k) - \bar{X}(T_s))^2} \sqrt{\sum_{k=T_s+1}^K (Y(k) - \bar{Y}(T_s))^2}}$$

where

$$\begin{aligned} \bar{X}(T_s) &= \frac{1}{K-T_s} \sum_{k=1}^{K-T_s} X(k) \\ \bar{Y}(T_s) &= \frac{1}{K-T_s} \sum_{k=T_s+1}^K Y(k) \end{aligned}$$

Then the optimal time shift T_s^* is defined as the time shift that maximizes the absolute value of the correlation coefficient r .

Given that $r(T_s) \neq 0$, it is necessary to determine, with enough confidence, whether $\rho(T_s) \neq 0$, that is, whether there exists a *nonvanishing* correlation between $X(k)$ and $Y(k+T_s)$. This confidence analysis is based on the fact that, when $X(k), Y(k+T_s)$ are independently ($\rho = 0$) Gauss distributed, the variable

$$t = r \frac{\sqrt{K-T_s-2}}{\sqrt{1-r^2}}$$

approximately follows a t -distribution with $K-T_s-2$ degrees of freedom [5].² From this, a lower bound on $|t|$, hence on $|r|$, can be found such that $\rho \neq 0$ with a prescribed level of confidence.

²Also recall that the sample distribution of $\frac{1}{2} \log \frac{1+r}{1-r}$ is approximately Gaussian with mean $\frac{1}{2} \log \frac{1+\rho}{1-\rho}$.

Existence of a correlation between $X(k)$ and $Y(k + T_s)$ reveals a regression relation that could take either form

$$\begin{aligned} Y(k + T_s) &= aX(k) + b \\ X(k) &= a'Y(k + T_s) + b' \end{aligned}$$

Since $aa' = r^2$, the correlation does not assign a preference to either relation. Ultimately, what regression, if any, should be preferred depends on the behavior of $r(T_s)$ as a function of T_s . If $r(T_s)$ increases as T_s increases from 0, then the first one should be preferred, which indicates that X is the cause and Y is the effect. However, no such increase of $r(T_s)$ with T_s has been found, so that there is no objective preference for either regression. Specifically, $r(T_s)$ behaving as $\pm \cos \omega T_s$ on the subband signal indicates a stationary wave phenomenon.

3.2.1 correlation among raw signals

The problem is that the sEMG signal consists, notwithstanding various noise, of many “bursts” running up and down the spine. As such, statistical correlation analysis on the raw signals only establishes a *traveling* wave phenomenon, easily visualized by “following the burst.” However, taking the correlation between the raw signals at two different points, without preprocessing, sometimes results in a correlation that is a bit weak, does not show a very clear pattern, and as such is a bit hard to interpret. A way to increase the correlation is provided by wavelet filtering.

3.2.2 correlation among wavelet subband signals

To increase the correlation and to detect a coherent *stationary* wave phenomenon, it is necessary to restrict ourselves to some relevant component of the signal, which is most easily identified as a selected subband of the Daubechies DB_3 wavelet decomposition. Besides, the same wavelet decomposition allows some filtering: The signal during NSA care is wavelet decomposed and compared with the wavelet decomposition of a control signal recorded when the wave phenomenon is absent. This indicates that only part of the wavelet decomposition was really relevant to the NSA wave phenomenon.

After trial and error, the Daubechies wavelet of order 3 (“ DB_3 ”) appeared to be the most appropriate. This finding is fully consistent with [23], where DB_3 was also adopted, for the slightly different reason that this wavelet mimics the single Motor Unit Action Potential (MUAP) detected by the electrodes. Another reason why the wavelet analysis works well is that the sEMG signal generated by NSA exhibits *some* self-similarity with a Hurst parameter between 0.51 and 0.55.

The signal was dyadic decomposed down to 8 levels as

$$\begin{aligned} X(k) &= D_1(k) + A_1(k) \\ X(k) &= D_1(k) + D_2(k) + A_2(k) \end{aligned}$$

$$\begin{aligned} & \vdots \quad \vdots \\ X(k) &= \sum_{i=1}^7 D_i(k) + D_8(k) + A_8(k) \end{aligned}$$

where D stands for “details” (or high resolution) and A stands for “approximation” (or low resolution). More specifically, if $\{\psi_{mn}(k) = 2^{-m/2}\psi(2^{-m}k - n)\}$ denote the orthonormal wavelet with m the resolution and n the shift and ψ the Daubechies function, the signal has representation

$$X(k) = \sum_{m,n} c_{mn} \psi_{mn}(k)$$

and the above decomposition reads:

$$\begin{aligned} X(k) &= \sum_n c_{1n} \psi_{1n}(k) + \sum_{m>1} \sum_n c_{mn} \psi_{mn}(k) \\ X(k) &= D_1(k) + \sum_n c_{2n} \psi_{2n}(k) + \sum_{m>2} \sum_n c_{mn} \psi_{mn}(k) \\ & \vdots \quad \vdots \\ X(k) &= \sum_{i=1}^7 D_i(k) + \sum_n c_{8n} \psi_{8n}(k) + \sum_{m>8} \sum_n c_{mn} \psi_{mn}(k) \end{aligned}$$

It turns out that the D_8 subband signal has very good correlation properties. To understand its spatial correlation properties, we write it as

$$u(x, k) = \sum_n c_{8,n}(x) \psi_{8,n}(k)$$

Clearly, the $c_{8,n}$ coefficients are patient specific. From the above decomposition, the computed correlation is

$$\begin{aligned} \frac{\overline{u(x_1, k)u(x_2, k + T_s)}}{\|u(x_1, \cdot)\| \cdot \|u(x_2, \cdot)\|} &= \\ \sum_{n_1, n_2} \frac{c_{8,n_1}(x_1)c_{8,n_2}(x_2)}{\sqrt{\sum_{n_1} c_{8,n_1}^2(x_1) \sum_{n_2} c_{8,n_2}^2(x_2)}} \overline{\psi_{8,n_1}(k)\psi_{8,n_2}(k + T_s)} & \quad (1) \end{aligned}$$

Clearly, this correlation has a patient specific component, because of the first factor in the right hand side, but it also has a wavelet specific component, because of the second factor in the right hand side. Now remember that n_2 is a delay which combines with T_s , so that by orthogonality the double sum reduces to a sum along a parallel to the diagonal, viz., $n_2 + 2^{-m}T_s = n_1$, so that the above reduces to

$$\frac{\overline{u(x_1, k)u(x_2, k + T_s)}}{\|u(x_1, \cdot)\| \cdot \|u(x_2, \cdot)\|} = \sum_{n_1} \frac{c_{8,n_1}(x_1)c_{8,n_1-2^{-m}T_s}(x_2)}{\sqrt{\sum_{n_1} c_{8,n_1}^2(x_1) \sum_{n_2} c_{8,n_2}^2(x_2)}} \quad (2)$$

4 spatio-temporal analysis of signals collected on baseline subjects

sEMG signals were collected on volunteering research subjects, in the protocol described in Section 5.2.

4.1 canonical correlation analysis of sEMG signals

The relationship between the time shift T_s and the past/future mutual information between signals recorded at two different points on the research subject BL99 (Level 2) was derived via canonical correlation analysis. The results when X is the sacral signal and Y the lumbar, thoracic, or cervical signal are shown in Figure 2-5, respectively.

The mutual information between the sacrum signal X and the other signals Y is a function of T_s , first increasing, then reaching a maximum for $T_s > 0$, and then decreasing. More specifically, from Figures 2 and 4, it appears that the electrophysiological phenomenon takes 30 sample points (15 msec.) to travel from the sacrum to the neck and 10-20 sample points (5-10 msec.) to travel from the sacrum to the lumbar spine, respectively. (A problem is that Figure 3 indicates that the wave takes 6 sample points (3 msec.) to go from the sacrum to the thorax, which is hard to reconcile with the previous traveling times, unless there exists some more direct nervous pathway from the sacrum to the thorax?) Putting on the side the thorax data, this analysis indicates that the sacrum area is the excitation, or the source of the wave, and that the lumbar, thoracic, and cervical signals are delayed versions of the sacral signal, therefore establishing a traveling wave pattern from the sacrum to the neck. That the sacrum is the excitation, or the cause, is justified by the fact that some research subjects experience more pronounced sacral than cervical oscillations.

Observe that the above traveling wave analysis reveals a electrophysiological propagation speed of roughly 100 m/sec., which is consistent with accepted figures [26, p. 59].

4.2 correlation analysis of sEMG phenomena

4.2.1 raw sEMG data signal

For the BL04 research subject, the computed correlation coefficients between random variables at various points and for various time-shifts are shown in the plots of Figures 6-9.

First, the correlation between the sEMG random variable at a point and the time-shifted random variable *at the same point* is relevant to the dynamics of this signal at that point and shows a unsurprising oscillatory behavior.

When it comes to the correlation between *two different points*, we can already perceive a pattern: Across Figures 6-9, observe that, for $T_s = 0$, there is opposite phase between, on the one hand, the neck random variable and, on the other hand, the thorax, lumbar spine, and sacrum random variables.

4.2.2 wavelet subband sEMG signal

In order to exhibit better correlation (hence higher confidence) and a more coherent phase pattern, we basically redo the same analysis but on the D_8 subband signal.

For both research subjects BL04 and Q04, all control and NSA signals were dyadic decomposed down to 8 levels with the Daubechies wavelet function [7, 25, 6] of order 3. By comparing the control and NSA wave signals (see Fig. 10), it becomes evident that the signals in A_8 are just base line drifting or low frequency noises (long term evolution) and as such are signals of no interest; neither are the signals in the D_1 to D_5 subbands of interest, because there is no difference between the test and the NSA signals and as such these signals consists mainly of high frequency noise. On the other hand, it is evident that the D_6, D_7, D_8 components are of more interest, because there is now a sizable difference between the test and NSA signals. Also, observe the marked “wavelet packets” in the D_7, D_8 subband signals, which are bursting phenomena running up and down the spine and establishing a “stationary” wave pattern. While a correlation analysis on D_7 could be carried out, we selected the D_8 signal, because it showed the better correlation properties.

The confidence level was set to 99%, meaning that the correlation is significant whenever the $r(T_s)$ versus T_s curve is outside the horizontal band bounded by the two lines parallel to the T_s axis. The time delay between each signals is around 100-150 samples points.

For the baseline subject BL04, the results of the correlation analysis of the D_8 subband signals for various time-shifts are shown in the plots of Figures 11-14. Observe that the curves are well outside the “slit” along the T_s axis, indicating a 99% confidence in the correlation.

Most importantly, observe the consistent phase pattern, with “zero crossing nodes,” much more pronounced than in the previous approach. (A “zero crossing node” is defined as a point where all four $r(T_s)$ versus T_s curves cross the $r = 0$ axis.)

If, in Equation 2, we set $x_1 = x_2 = x$, then the correlation becomes

$$r(T_s) = \frac{\sum_n c_{8,n}(x)c_{8,n-2^{-m}T_s}(x)}{\sum_n c_{8,n}^2(x)}$$

which vanishes for $T_s = 40$ samples points, etc. This gives an indication of *the frequency of the oscillation at the point x , or at any other point along the spine for that matter.*

Next, setting $T_s = 0$ in Equation 2 yields

$$r(T_s) = \frac{\sum_n c_{8,n}(x_1)c_{8,n}(x_2)}{\sqrt{\sum_{n_1} c_{8,n_1}^2(x_1) \sum_{n_2} c_{8,n_2}^2(x_2)}}$$

which obviously from the diagrams changes sign. Therefore, there exists at least one point x_* where the above vanishes, viz.,

$$\sum_n c_{8,n}(x_*)c_{8,n}(x_*) = \|c_{8,\cdot}(x_*)\|^2 = 0$$

which indicates existence of a *mode shape node* at x_* . Clearly, there exists such a node somewhere between the neck electrode and the thoracic electrode. We further conjecture that there are no waveform nodes between the thorax and the sacrum, because changes in the waveform signs between the thorax and the sacrum appear inconsistent with the kinematics of the spine. That there exists a waveform node between the neck electrode and the thorax electrode can be justified by the kinematic flexibility of the neck.

Clearly, all of the above indicates a stationary wave phenomenon.

5 clinical application: regeneration in the Central Nervous System

Here, we perform the spatio-temporal correlation analysis on a quadriplegic research subject.

5.1 problem

The problem is two-fold. First, to confirm that a quadriplegic patient who had sustained a C5 injury responds to NSA care in such a way as to exhibit the NSA wave. Second, to show evidence of some spinal cord regeneration.

5.2 methods

To record sEMG signals, ungelled, noninvasive electrodes were placed at cervical, thoracic, lumbar, and sacral positions along the spine. The unfiltered sEMG data was collected over a bandwidth of 10-500 Hz by an InsightTM Millennium machine, converted to digital format with a 16 bit precision DAS16/16 PCMCIA card, and stored on a PC compatible laptop computer. FFT analysis of the signals revealed a peak at about 125 cycles/sec.

The data used here was collected in two different sessions:

1. S99: An older recording session in 1999, at a sampling frequency of 2000 samples/sec., using a baseline subject BL99.
2. S04: A recent recording session in 2004, at a sampling frequency of 4000 samples/sec., using a baseline subject BL04 and a quadriplegic subject Q04. The latter subject had a swimming pool accident, dove in deep end of pool with only 4 feet of water, sustained C-5 spinal cord injury (similar to the case reported in [18]), C-5 vertebrae was surgically removed and replaced with a titanium plate from C-4 to C-6.

All research subjects had previously signed the *Informed Consent Form* in a protocol approved by the Institutional Review Board (IRB) of the University of Southern California.

In order to assess noise or other irrelevant pattern during S04, before entrainment but with the research subject in the same position and with the same

wiring as during entrainment, time-series signals were recorded to be used as control or testing signals. Then, keeping the same experimental environment, the subject was entrained and the NSA wave was recorded.

The “lag” L was systematically set to 25.

5.3 results

The same correlation analysis, but on the quadriplegic subject Q04, is shown in Figures 15-18.

First, observe that all correlations involving the neck signals are weak, as can be anticipated from the neck injury, *but they are still in the 99% confidence interval. This positive correlation between signals on both sides of the spinal cord injury indicates that nerve impulses pass through, or peripherally around, the injury area, hence indicating some partial motor recovery.*

Second, the stationary wave pattern does not appear as clearly as for the baseline subject, as can be seen by the defective “zero crossing nodes.” However, the thoracic, lumbar, and sacral plots (Fig. 16, 17, 18, resp.) do show zero crossing nodes, *if we remove the neck signals from those plots. It therefore appear that there is some stationary pattern involving the thorax, lumbar spine, and sacrum, but not involving the neck.*

To allow for an easy comparison between the baseline and quadriplegic subjects, the correlation curves of Fig. 11-18 are merged into Fig. 19, with the baseline subject curves on the left and the quadriplegic subject curves on the right. The first and most striking difference between the baseline subject (Fig 11) and the quadriplegic subject (Fig 15) is a weaker correlation between, on the one hand, the neck and, on the other hand, the cervical, thoracic, lumbar or sacral signals, as can be anticipated because of the neck injury. Another striking difference is that, in the thoracic, lumbar and sacral plots of Fig. 19, the correlation involving the neck signal of the quadriplegic subject is off phase as compared with the baseline subject.

5.4 discussion

In conclusion, it appears that the stationary wave pattern cannot completely establish itself, because of the neck injury.

While there is considerable debate as to whether and how regeneration in the CNS occurs [18], this extra phase shift seems to indicate that the regeneration has happened via the periphery of the cord.

One can only speculate that, for a patient with a spinal injury around C5, the nervous activity generated by the cervical and sacral oscillators *on both sides of the spine injury* reconstructs, through Hebb’s law, synaptic strengths in the periphery of the injury, thereby achieving some “rewiring.”

6 Sensory-motor instability or central pattern generator?

By Alf Breig’s neurosurgical model, the cervical and sacral oscillations appear to be result of sensory-motor instabilities [13]. In fact, based on our overall experience of visual observation of the wave and sEMG analysis, the most likely nervous pathways can be traced as shown in Figures 20, 21. While some research in migraine headache and subaracnoid hemorrhage [16] reveals pathways from the dural mechanoreceptors to the trigeminal ganglion, which itself innervates the trapezius shoulder muscle, these pathways do not appear to be essential to sustain the wave phenomenon, since a quadriplegic patient was able to experience the NSA wave.

On the other hand, the NSA wave definitely has some external resemblance with the swimmeret motion [19], which points to a Central Pattern Generator (CPG). The CPG theory is further confirmed by the quadriplegic case study, which points to nervous pathways entirely within the spine. A comparison between the frequencies of oscillation associated with CPG and the NSA wave phenomenon experienced by the quadriplegic patient leads to an insight in the connection between CPG and the phenomenon under study. Autonomous activity of the CPG through the positive feedback received from the stretch receptors at low gain yields a CPG frequency of 20 Hz. Positive feedback at a medium gain yields a CPG frequency of 40 Hz. In the presence of positive feedback, the CPG functions autonomously in a large range of gain values where the CPG frequency scales practically linearly with the gain, resulting in a CPG frequency of 60 Hz at high gain [21]. The quadriplegic patient had been under NSA care for about one year prior to the sEMG recording and based upon hebbian learning the neural network has acquired a high gain. The electrophysiological wave takes 15 milliseconds to travel from the sacrum to the neck [10], at a frequency of 66.67 Hz which matches closely with that of the CPG frequency at high gain.

Sensory-motor instability or Central Pattern Generator? This dichotomy can probably be resolved by the observation that both of them are involved in the NSA wave. The sensory-motor instability which elicits the neck oscillations appears to be the Hebbian learning of the Central Pattern Generator. Indeed, when the research subject reaches the higher levels of care, neck manipulation and the resulting vertebra oscillations no longer seem to be necessary, as the NSA wave is nearly spontaneous.

7 Conclusions

Using statistical correlation techniques on the sEMG signals recorded at various points along the paraspinal muscles, the Network Spinal Analysis (NSA) wave phenomenon has been positively identified. This phenomenon is triggered by sensory-motor loops at the neck and at the sacrum, from where it propagates up and down the spine and reflects at the neck and at the sacrum. From the point of view of wave physics, the reflection of the wave calls for some “boundary

conditions,” which here are materialized by the dural-vertebral attachments. The uprunning and the downrunning waves somehow combine and “resonate,” consistently with the propagation speed and the properties of the “medium,” only at a specific subband of the Daubechies wavelet decomposition.

Probably the most mathematically challenging problem motivated by the above is the reconstruction of the partial differential equation of the wave, given the observed sEMG signals at various points.

On a quadriplegic subject, the resonance pattern allows Hebbian learning, which itself creates some partial CNS regeneration. But probably most important is the fact that a quadriplegic patient is able to experience the wave. This points to nervous pathways entirely within the spine, hence the existence of a CPG.

Probably the most challenging neurophysiological problem that this analysis has unveiled is a better understanding of CPG’s and how they are “learned” in the Hebbian sense by sensory-motor instabilities.

Acknowledgment

Many thanks to Dr. D. Epstein, Dr. R. Boone, and Dr. L. Stern for many helpful discussions.

References

- [1] S. Bohacek and E. A. Jonckheere. Chaotic modeling in network spinal analysis: Preliminary report: Nonlinear canonical correlation with alternating conditional expectation (ACE). *Journal of Vertebral Subluxation Research*, 2(4):188–195, December 1998.
- [2] A. Breig. *Adverse Mechanical Tension in the Central Nervous System*. John Wiley and Sons, New York, 1987.
- [3] A. Breig. *Skull Traction and Cervical Cord Injury: A New Approach to Improved Rehabilitation*. Springer Verlag, 1989. ISBN: 0387504141.
- [4] L. Breiman and J.H. Friedman. Estimating optimal transformations for multiple regression and correlation. *Journal of the American Statistical Association (JASA)*, 80:580–598, 1985.
- [5] M. G. Bulmer. *Principles of Statistics*. Dover, New York, 1979.
- [6] I. Daubechies. Orthonormal bases of compactly supported wavelets. *Communications on Pure and Applied Mathematics*, XLI:909–996, 1988.
- [7] I. Daubechies. *Ten lectures on wavelets*. CBMS-NSF Conference Series in Applied Mathematics. SIAM, 1992.

- [8] M. Grattarola, M. Ciappalone, F. Davide, S. Martinoira, M. (B.) Tedesco, N. Rosso, and A. Vato. Burst analysis of chemically stimulated spinal cord neuronal networks cultured on microelectrode arrays. Technical report, Neural and Bioelectronic Technologies group, Department of Biophysical and Electronic Engineering, University of Genoa, Italy, 2004.
- [9] E. A. Jonckheere and S. K. Bohacek. Chaotic modeling in network spinal analysis: Mathematical classification of level 1,2,3 patients. Technical report, University of Southern California, 2003. Available on line from the password protected web site of <http://eudoxus.usc.edu/CHAOS/nsa.html>.
- [10] E. A. Jonckheere and P. Lohsoonthorn. Spatio-temporal analysis of an electrophysiological wave phenomenon. In *International Symposium on the Mathematical Theory of Network and Systems (MTNS2004)*, Leuven, Belgium, 2004.
- [11] E. A. Jonckheere, P. Lohsoonthorn, and V. Mahajan. Chiro-sensor—an array of non-invasive sEMG electrodes. In J. D. Westwood et al., editor, *Medicine Meets Virtual Reality 13: The Magical Next Becomes the Medical Now*, volume 111 of *Technology and Informatics*. IOS Press, Amsterdam, Berlin, Oxford, Tokyo, Washington, D.C., 2005.
- [12] Edmond A. Jonckheere and Poonsuk Lohsoonthorn. Dynamic modeling of surface electromyographic activity during various spinal conditions. In *American Control Conference (ACC2003)*, pages 465–470, Denver, CO, June 4-6 2003. Session: Biomedical Applications, WA-13-3.
- [13] D. Kleinfeld, R. W. Berg, and S. M. O’Connor. Anatomical loops and their electrical dynamics in relation to whisking by rat. *Somatosensory & Motor Research*, 16(2):69–88, 1999.
- [14] N. Kopell. We got rythm: Dynamical systems of the nervous system. *Notice of the AMS*, 47(1):6–16, January 2000.
- [15] W. E. Larimore. Identification and filtering of nonlinear systems using canonical variate analysis. In M. Casdagli and S. Eubank, editors, *Nonlinear Modeling and Forecasting, SFI Studies in the Sciences of Complexity*, volume 12. Addison-Wesley, 1992.
- [16] D. Levy and A. Strassman. Mechanical response properties of A and C primary afferent neurons innervating the rat intracranial dura. *J. Neurophysiology*, 88:3021–3031, 2002.
- [17] P. Lohsoonthorn and E. A. Jonckheere. Nonlinear switching dynamics in surface electromyography of the spine. In *Physics and Control*, pages 277–282, St. Petersburg, Russia, August 21-23 2003.
- [18] J. W. McDonald, D. Becker, C. Sadowsky, J. A. Jane, T. E. Conturo, and L. Schultz. Late recovery following spinal cord injury. *J. Neurosurg (Spine 2)*, 97:252–265, 2002.

- [19] O. Haug Olsen and D. Murray-Smith. Quantifying periodic activity in central pattern generators: the crayfish swimmeret. *Journal of Neuroscience Methods*, 50:25–35, 1993.
- [20] M. Panjabi. The stabilizing system of the spine. part i. function, dysfunction, adaptation, and enhancement. *Journal of Spinal Disorders*, 5(4):383–389, 1992.
- [21] T. Sejnowski, C. Koch, and R. Douglas. A model of a single segment of the lamprey spinal cord. In *NSF Workshops on Neuromorphic Engineering*, page 21, Telluride, CO, 1997.
- [22] E. E. Selkurt. *Physiology*. Little, Brown and Company, Boston, 1971.
- [23] W.M. Sloboda and V.M. Zatsiorsky. Wavelet analysis of emg signals. In *Twenty-First Annual Meeting of the American Society of Biomechanics*, Clemson University, South Carolina, September 24-27 1997.
- [24] J.-J. E. Slotine, W. Wang, and K. El Rifai. Contraction analysis of synchronisation and desynchronisation in networks of nonlinearly coupled oscillators. In *Mathematical Theory of Networks and Systems (MTNS2004)*, Leuven, Belgium, July 5-9 2004. Mini Symposium on Mathematical Theory of Oscillations in Networks and Systems, WP-1.
- [25] G. Strang and T. Nguyen. *Wavelets and Filter Banks*. Wellesley-Cambridge, 1996.
- [26] R. F. Thompson. *The Brain*. W. H. Freeman, New York, 1993.
- [27] R. Warick and P. L. Williams, editors. *Gray's Anatomy*. W.B. Saunders Co., Philadelphia, 1973. 35th British Ed.

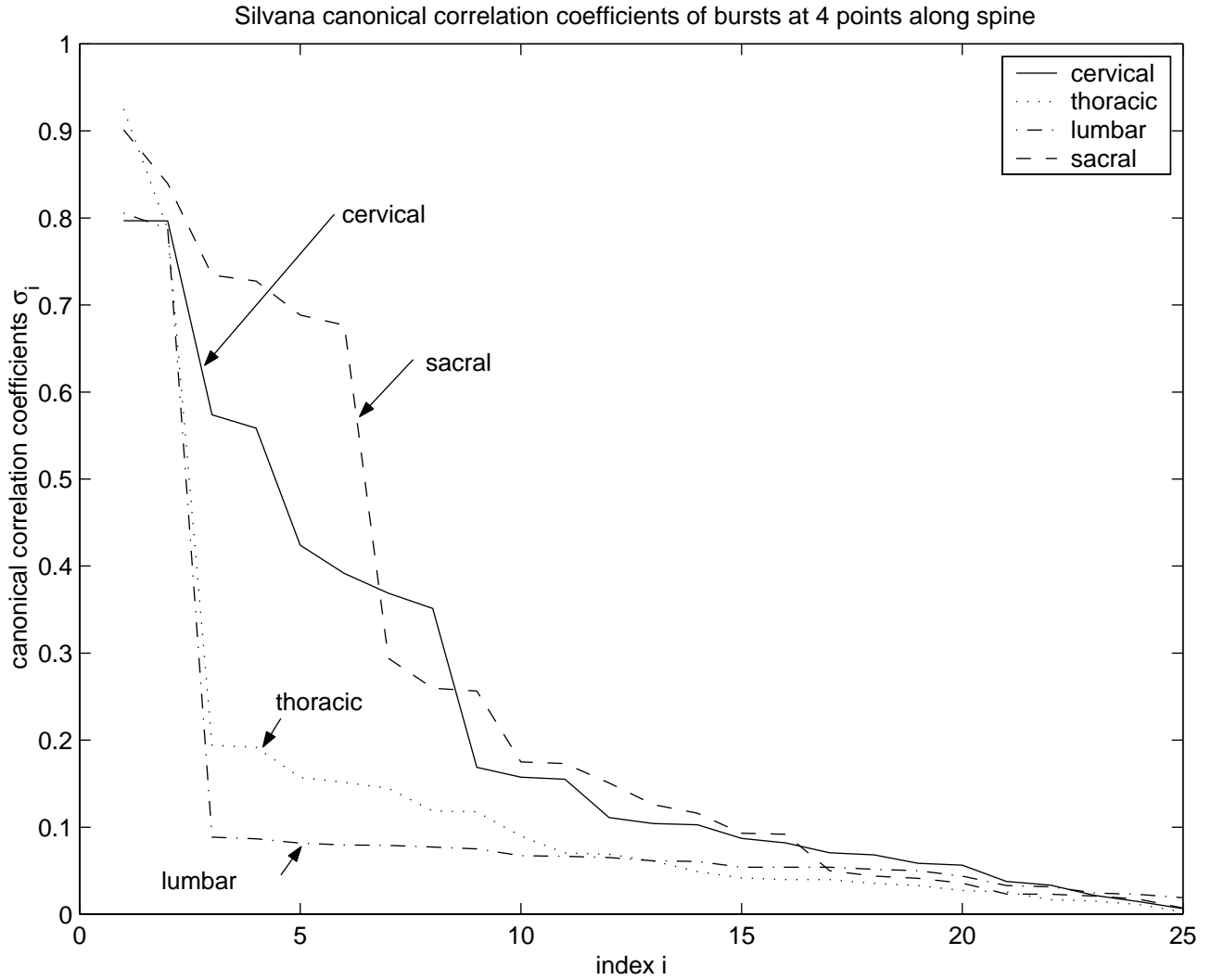


Figure 1: Canonical correlation coefficient sequences at the four points along the spine of a Level 2 research subject, revealing much higher order models at the cervical and sacral levels. Clearly, the cervical and sacral oscillators are engaged, and the chess-thoracic oscillator is about to be engaged.

Figure(13) Megin past/future mutual information between sacrum and neck

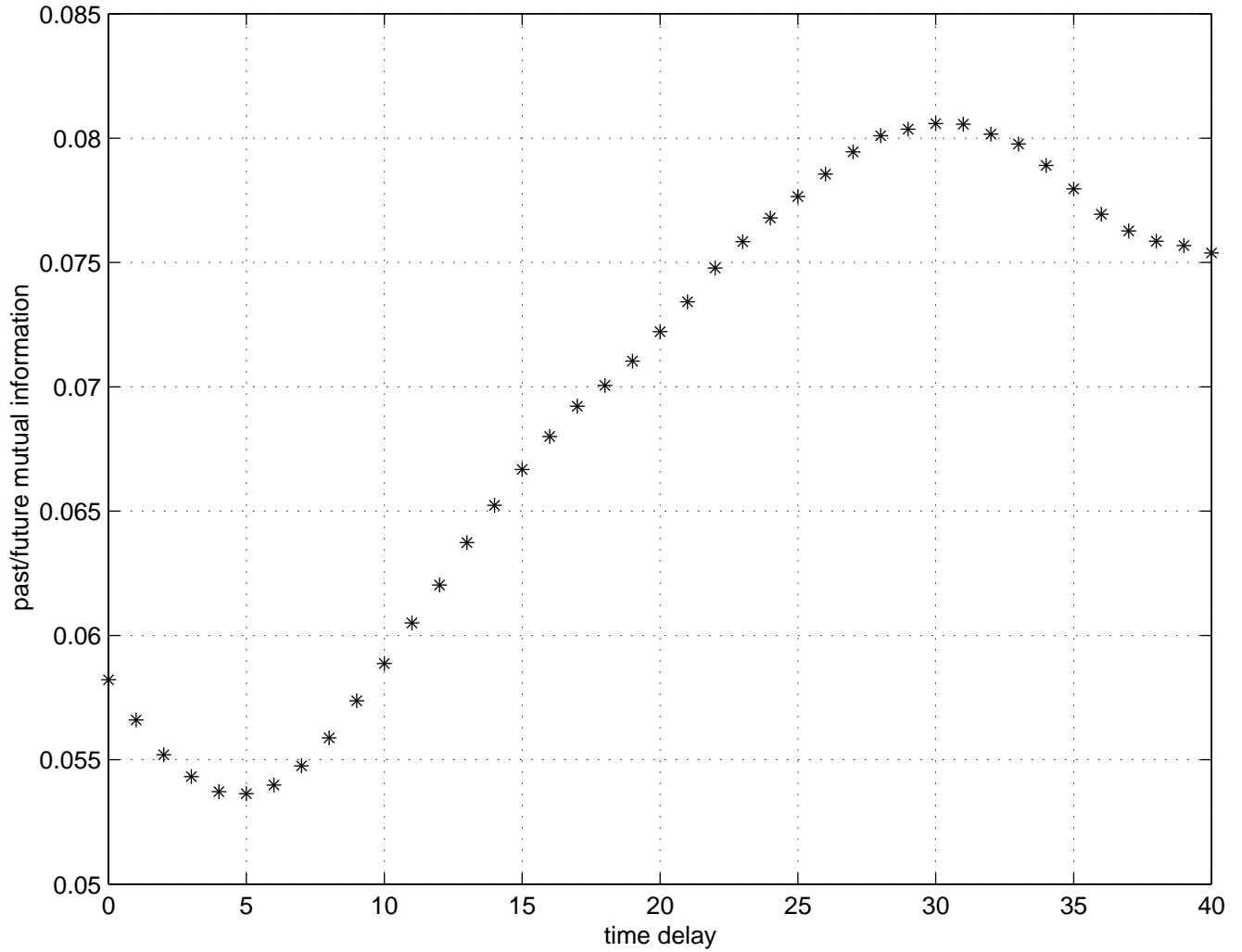


Figure 2: Mutual sacrum/neck information versus time-shift. Because the information reaches a maximum for $T_s > 0$, this plot establishes a traveling wave from the sacrum to the neck.

Figure(14) Megin past/future mutual information between sacrum and thorax

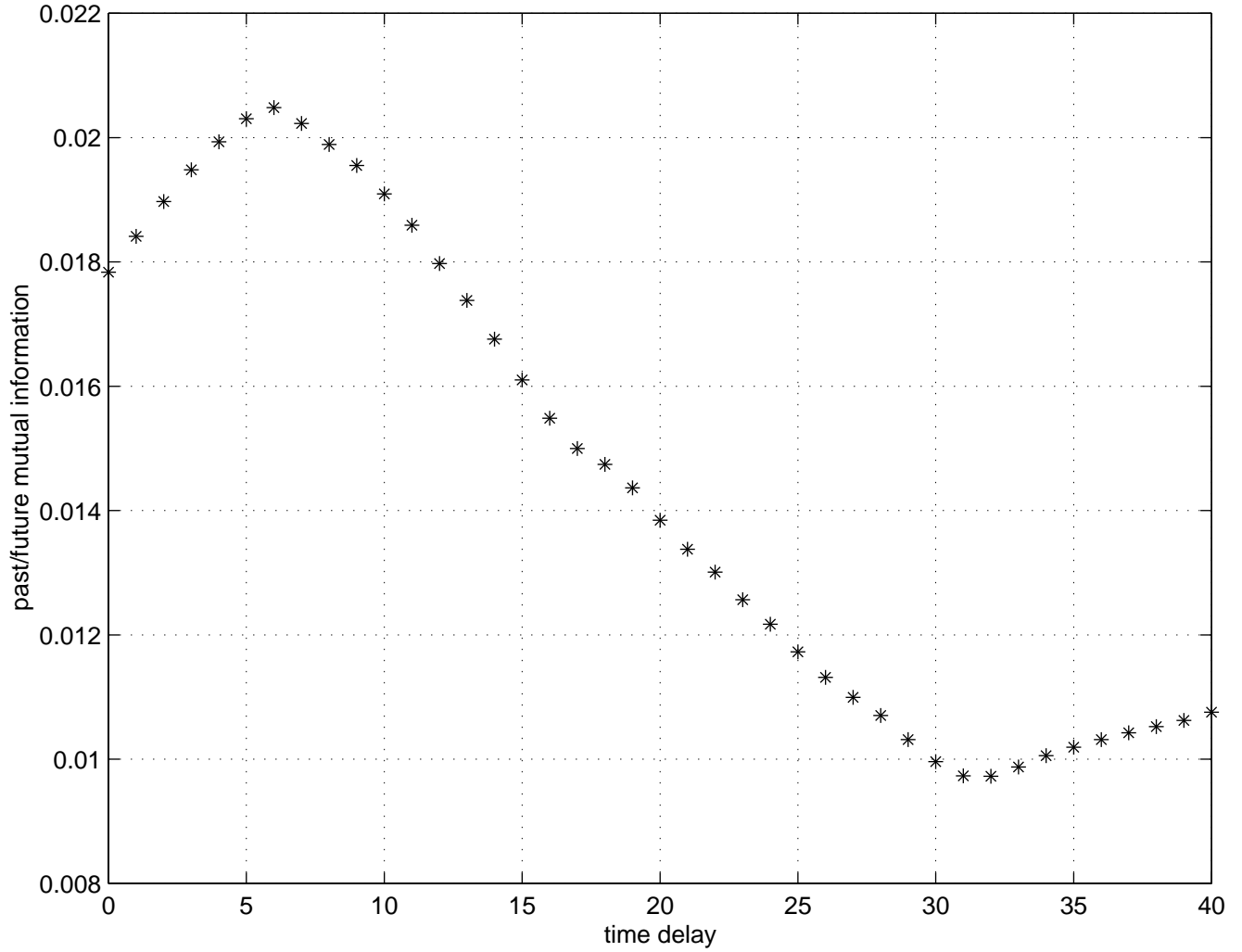


Figure 3: Mutual sacrum/thorax information versus time-shift. The fact that the information reaches a maximum for a small $T_s > 0$ seems (?) to reveal a fast traveling wave from the sacrum to the thorax.

Figure(15) Megin past/future mutual information between sacrum and lumbar spine

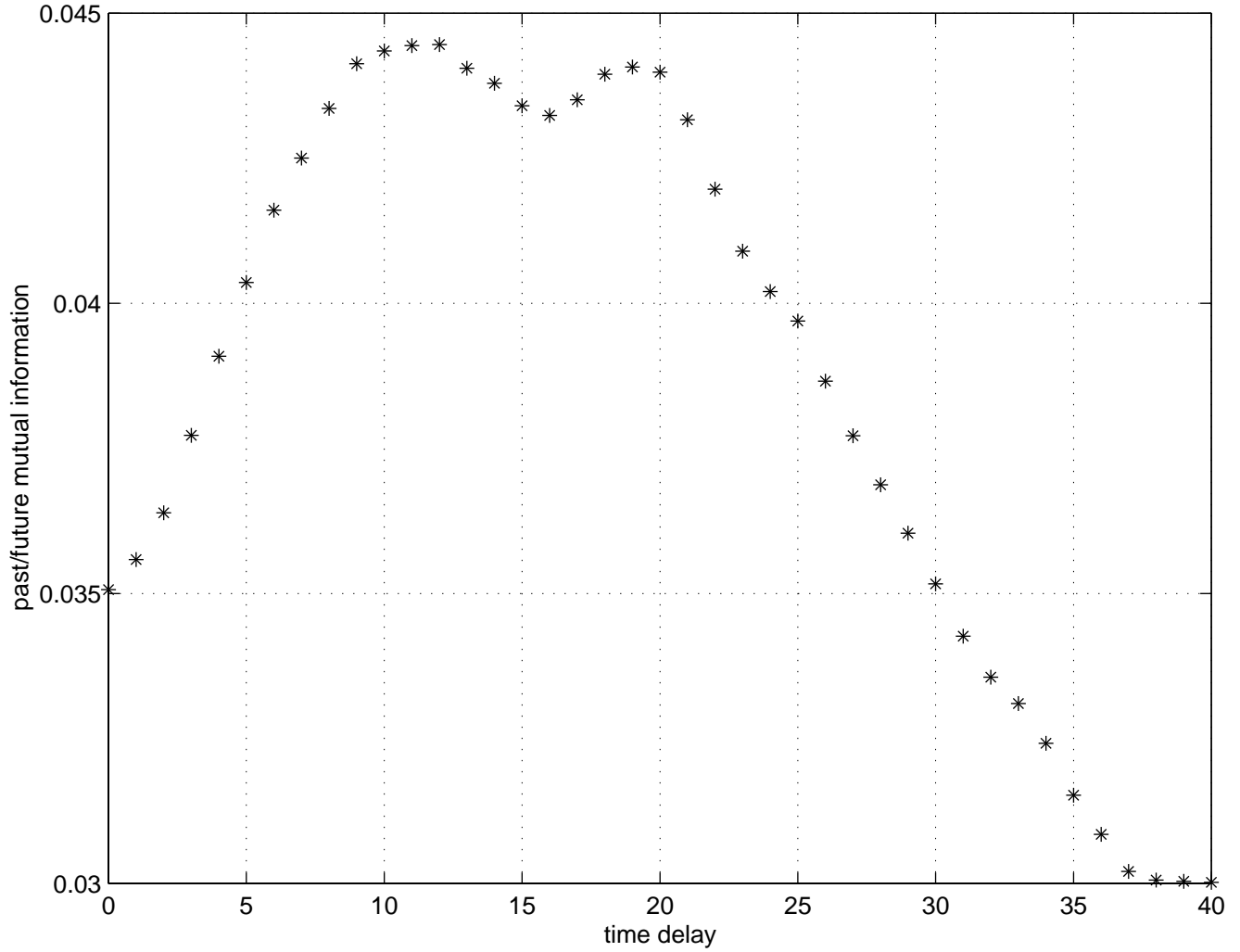


Figure 4: Mutual sacrum/lumbar spine information versus time-shift. Since the information reaches a maximum for $T_s > 0$, a traveling wave from the sacrum to the lumbar spine is established.

Figure(16) Megin past/future mutual information between sacrum and sacrum

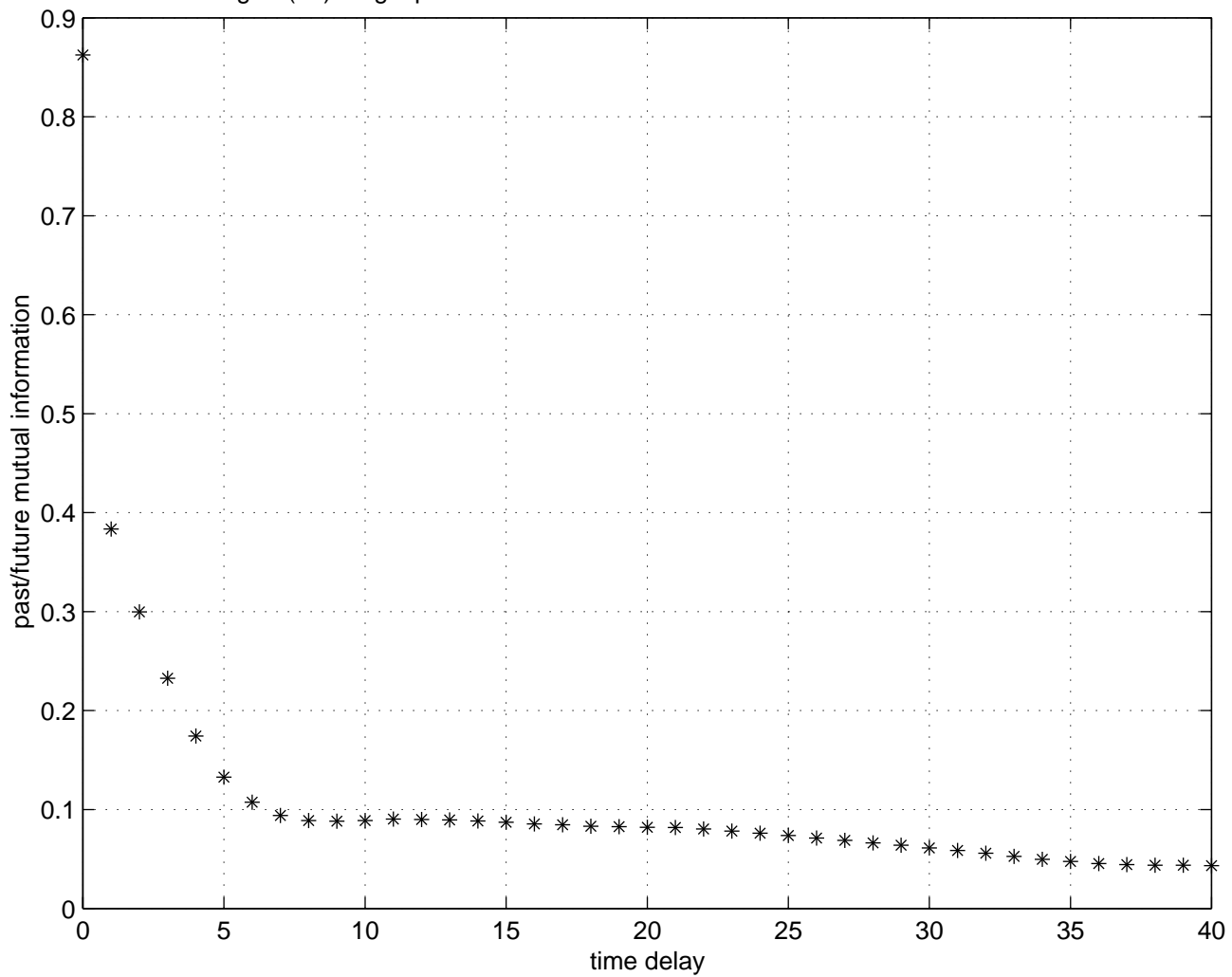


Figure 5: Mutual sacrum past/future information versus time-shift. Observe that the information is maximum for $T_s = 0$.

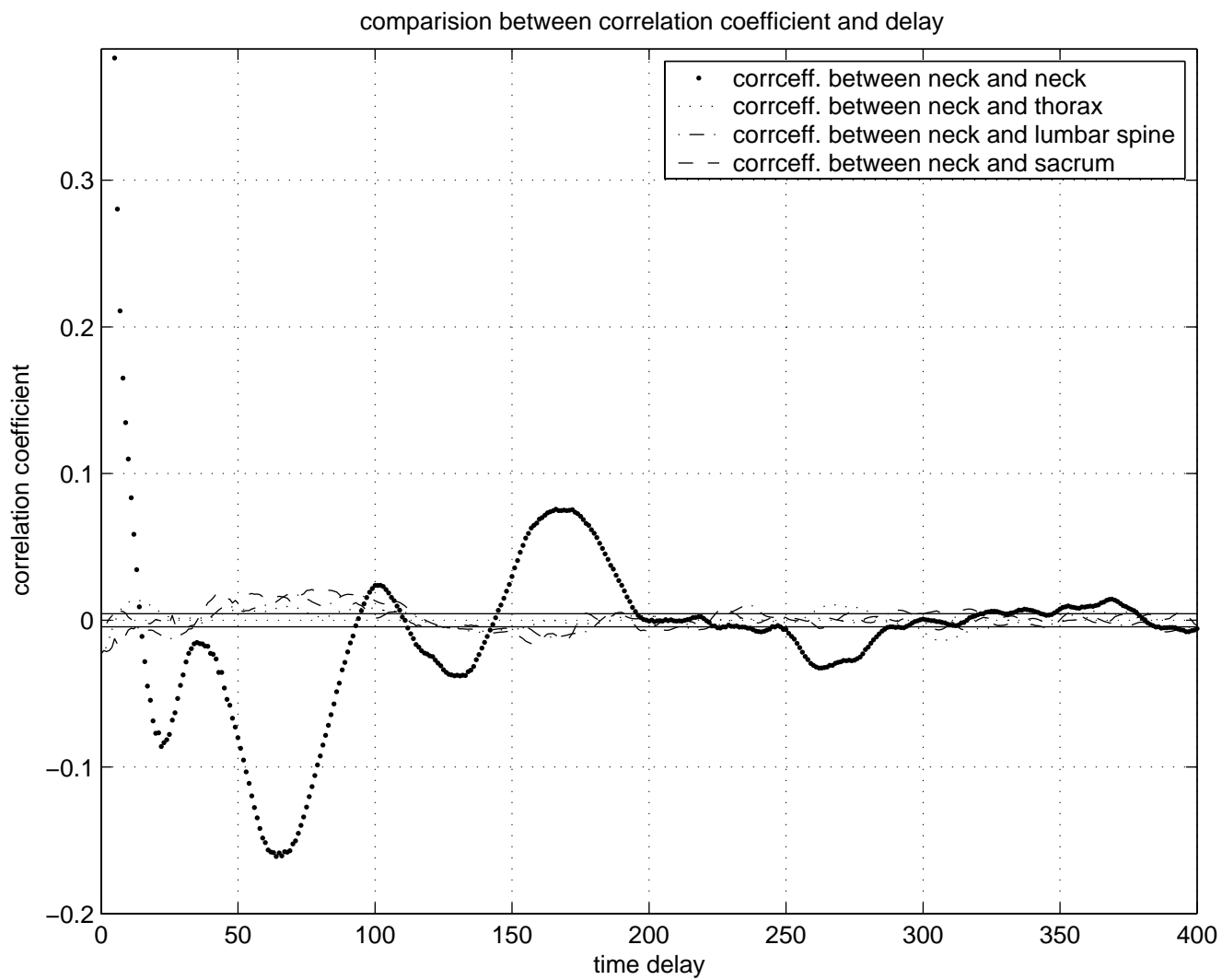


Figure 6: Correlation between neck and other signals for baseline subject BL04.

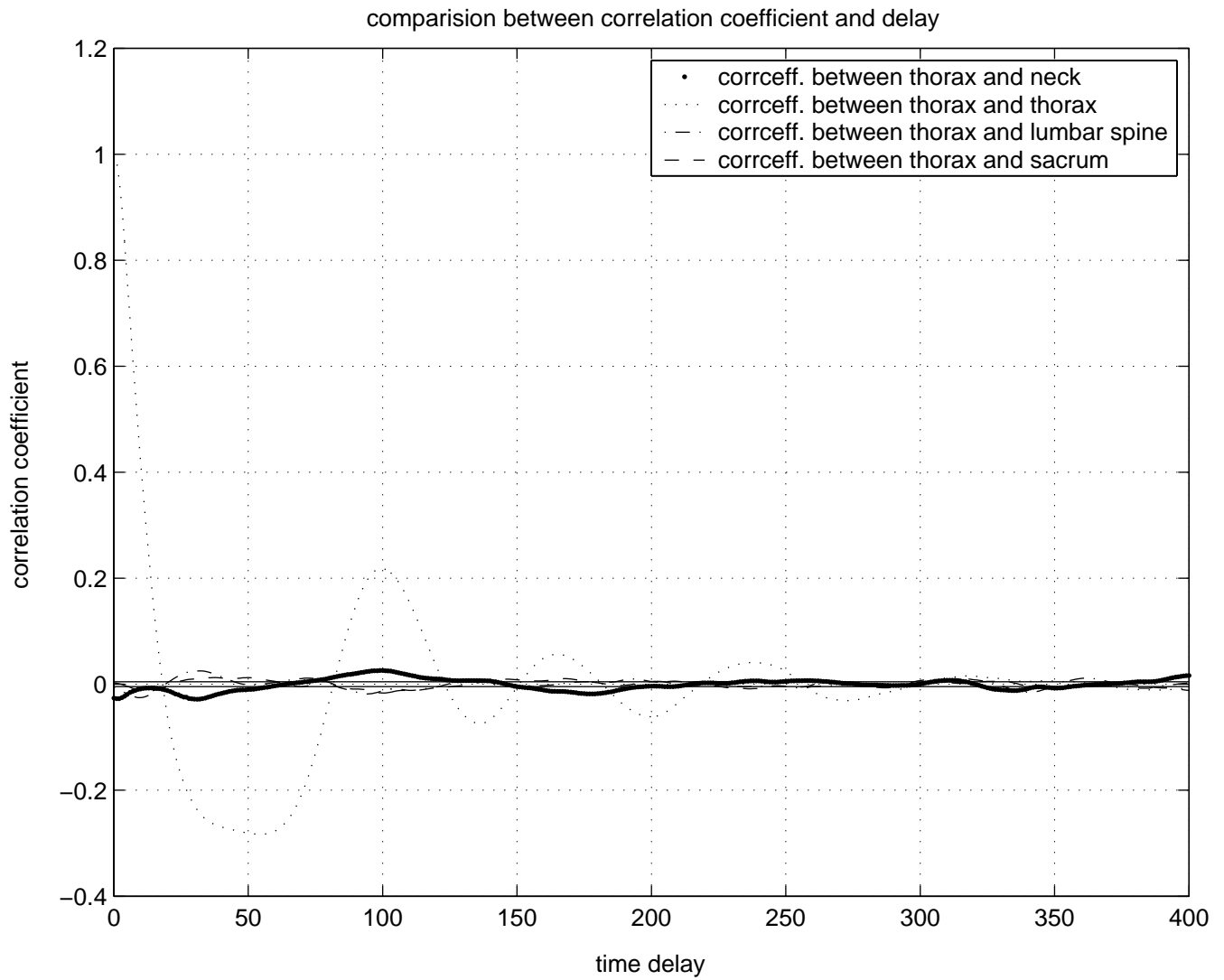


Figure 7: Correlation between thorax and other signals for baseline subject BL04.

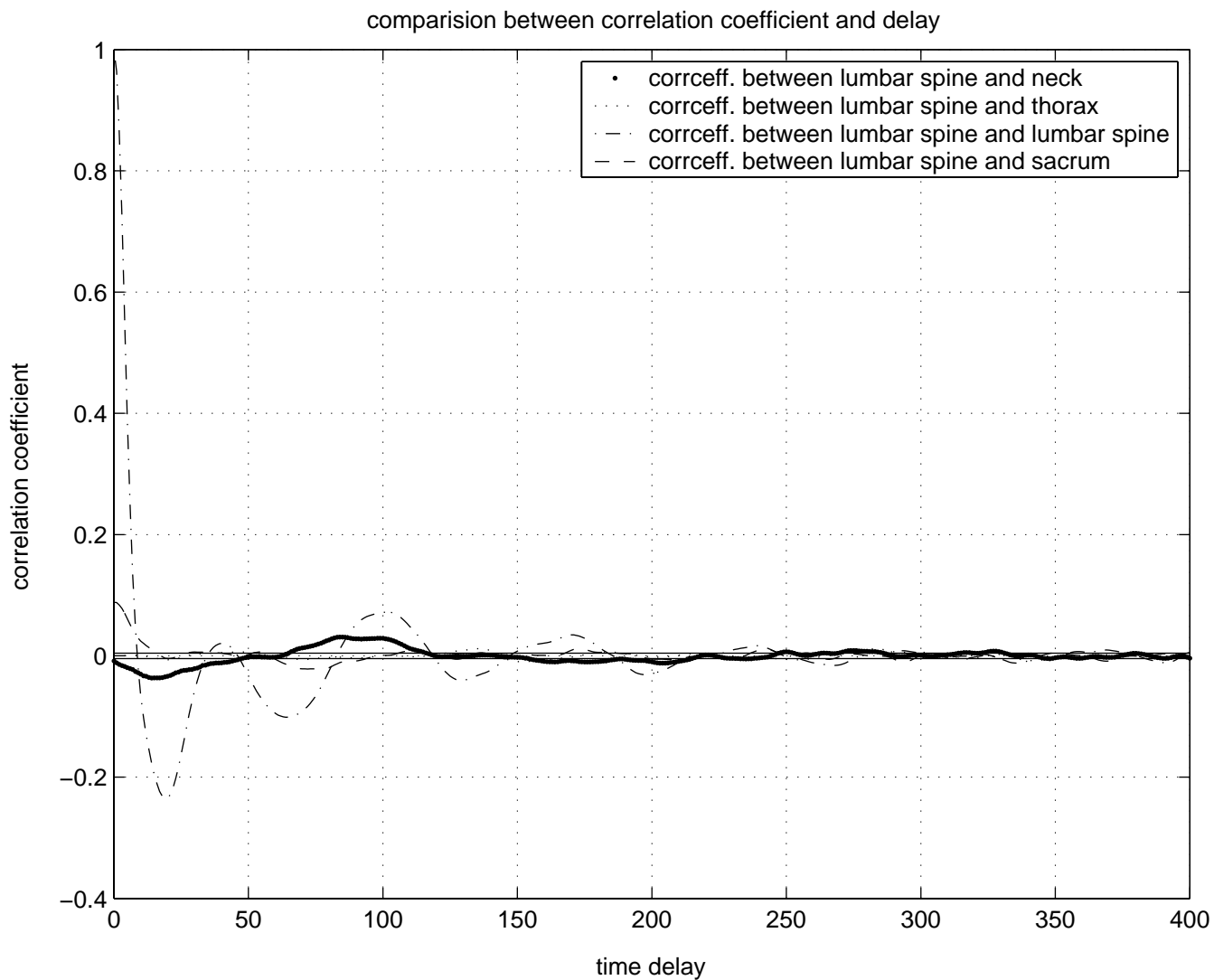


Figure 8: Correlation between lumbar spine and other signals for baseline subject BL04.

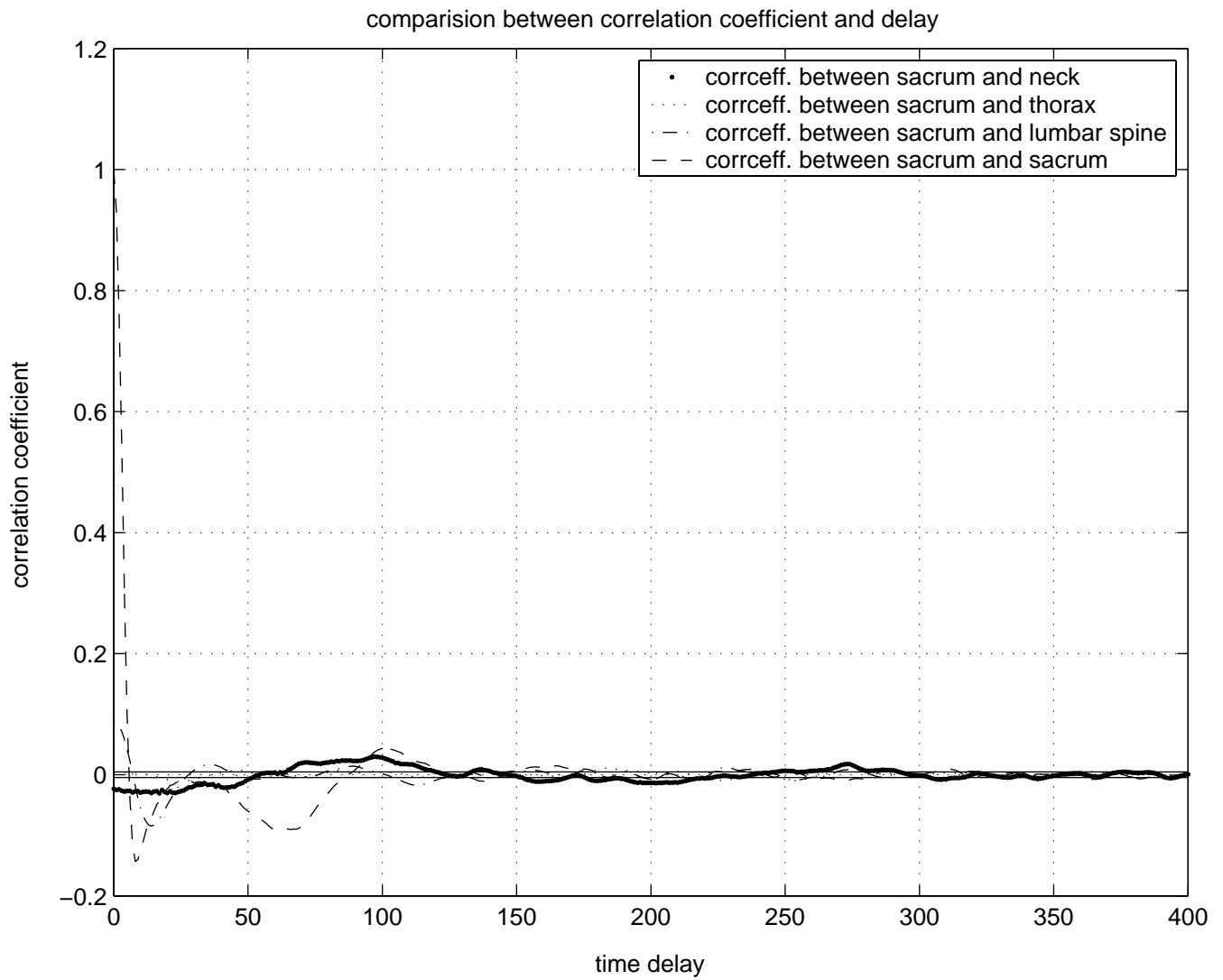


Figure 9: Correlation between sacral and other signals for baseline subject BL04.

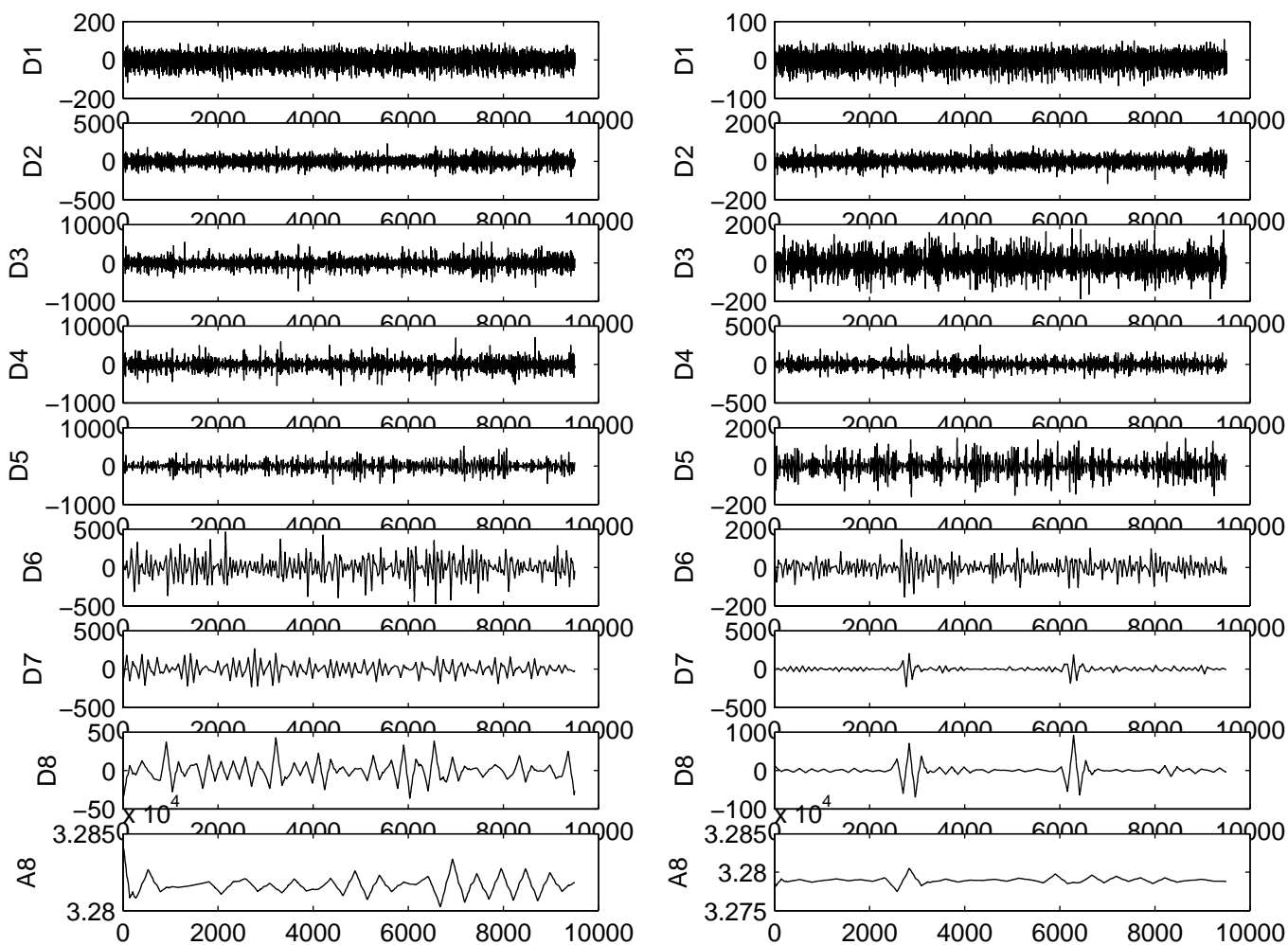


Figure 10: Comparison between wavelet decompositions of control signal (left) and NSA signal (right).

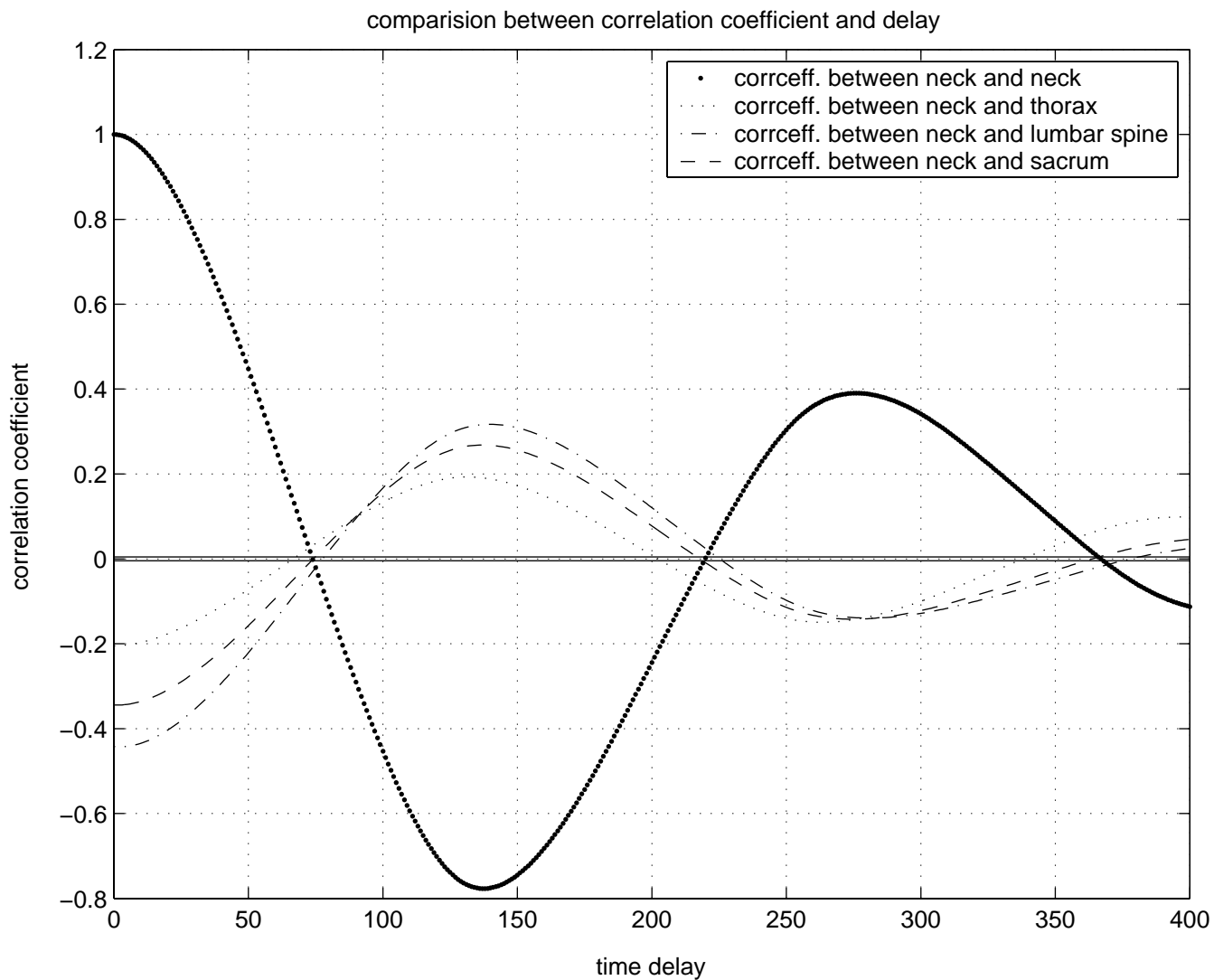


Figure 11: Correlation between subbands of neck and other signals for baseline subject BL04.

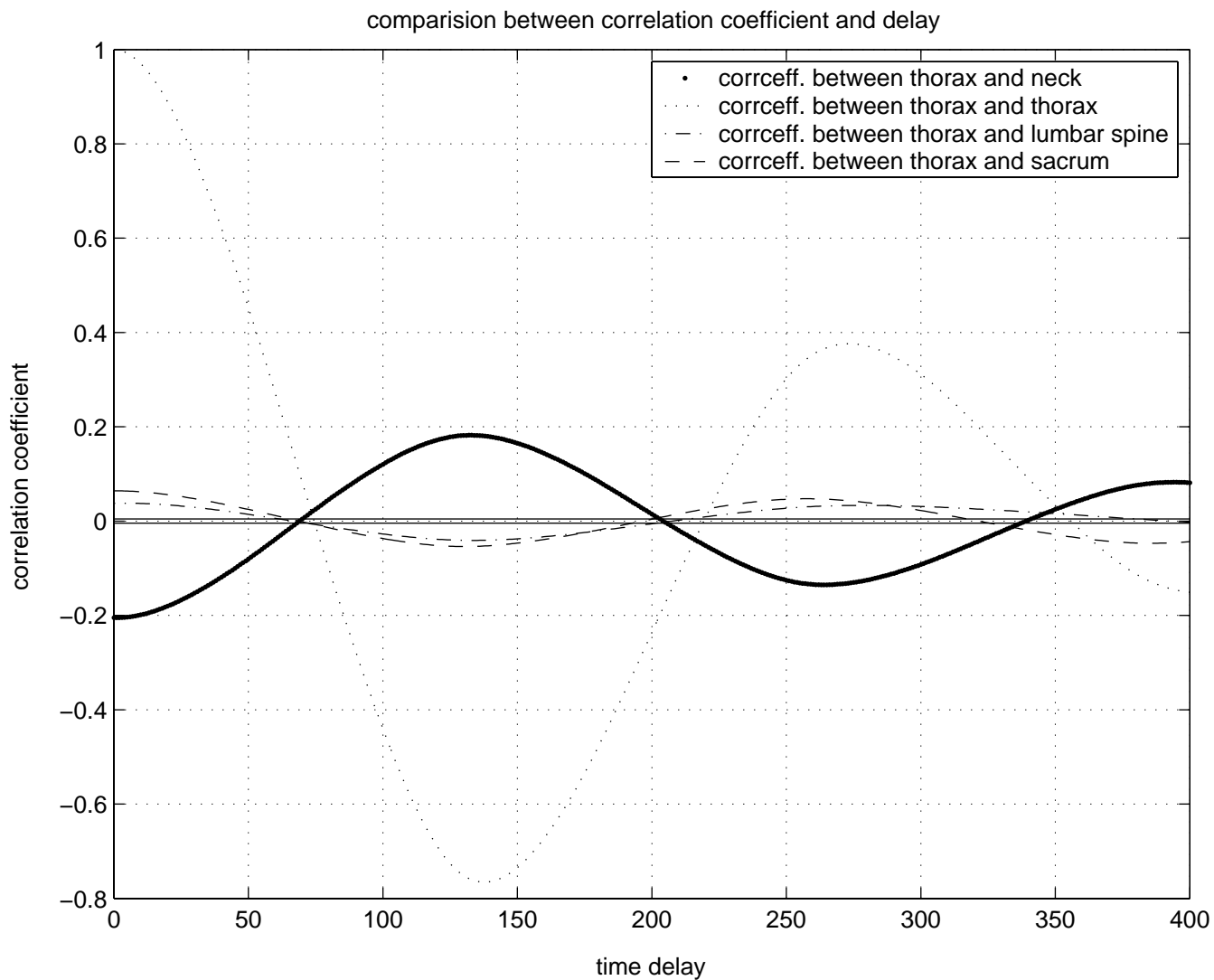


Figure 12: Correlation between subbands of thorax and other signals for baseline subject BL04.

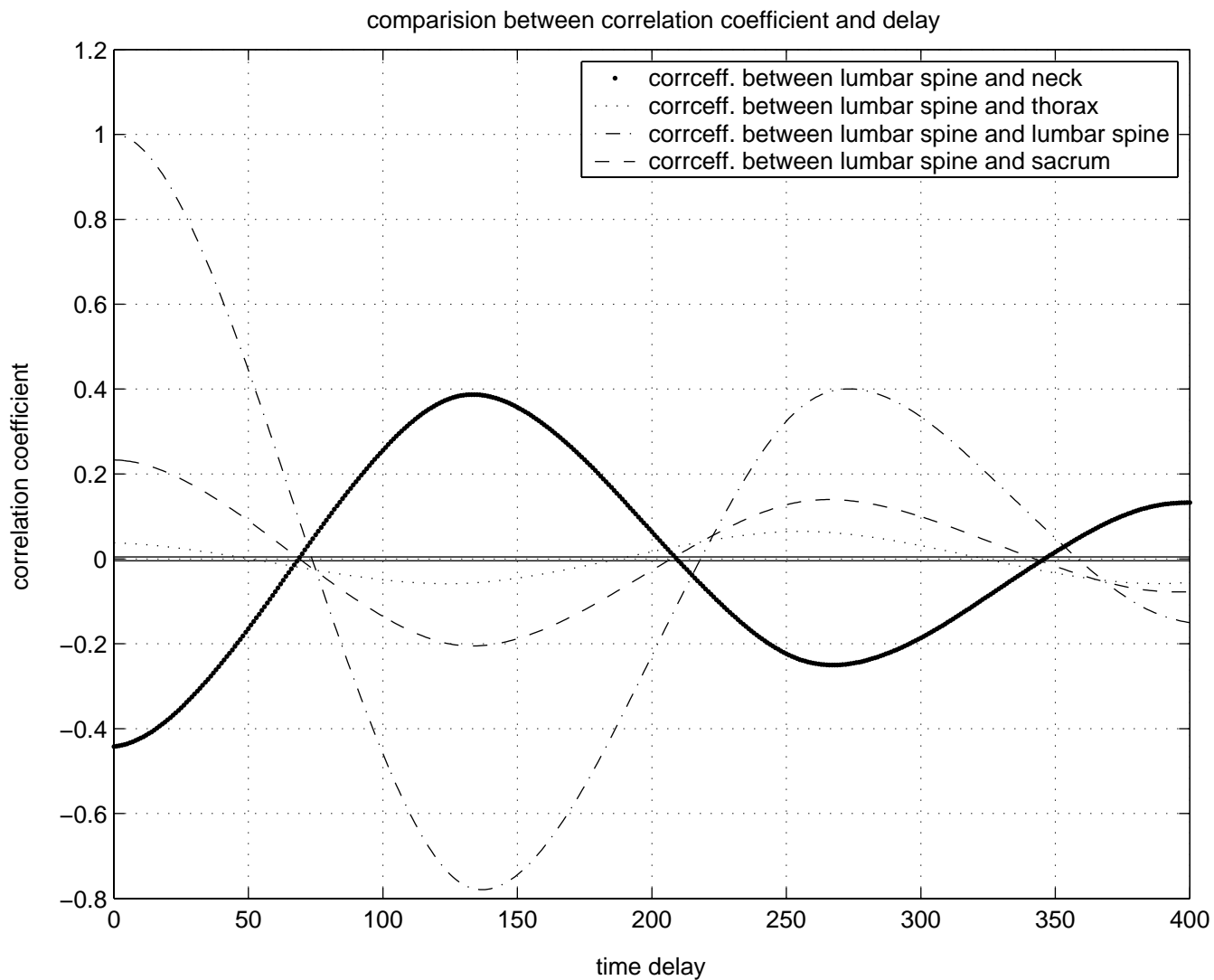


Figure 13: Correlation between subbands of lumbar spine and other signals for baseline subject BL04.

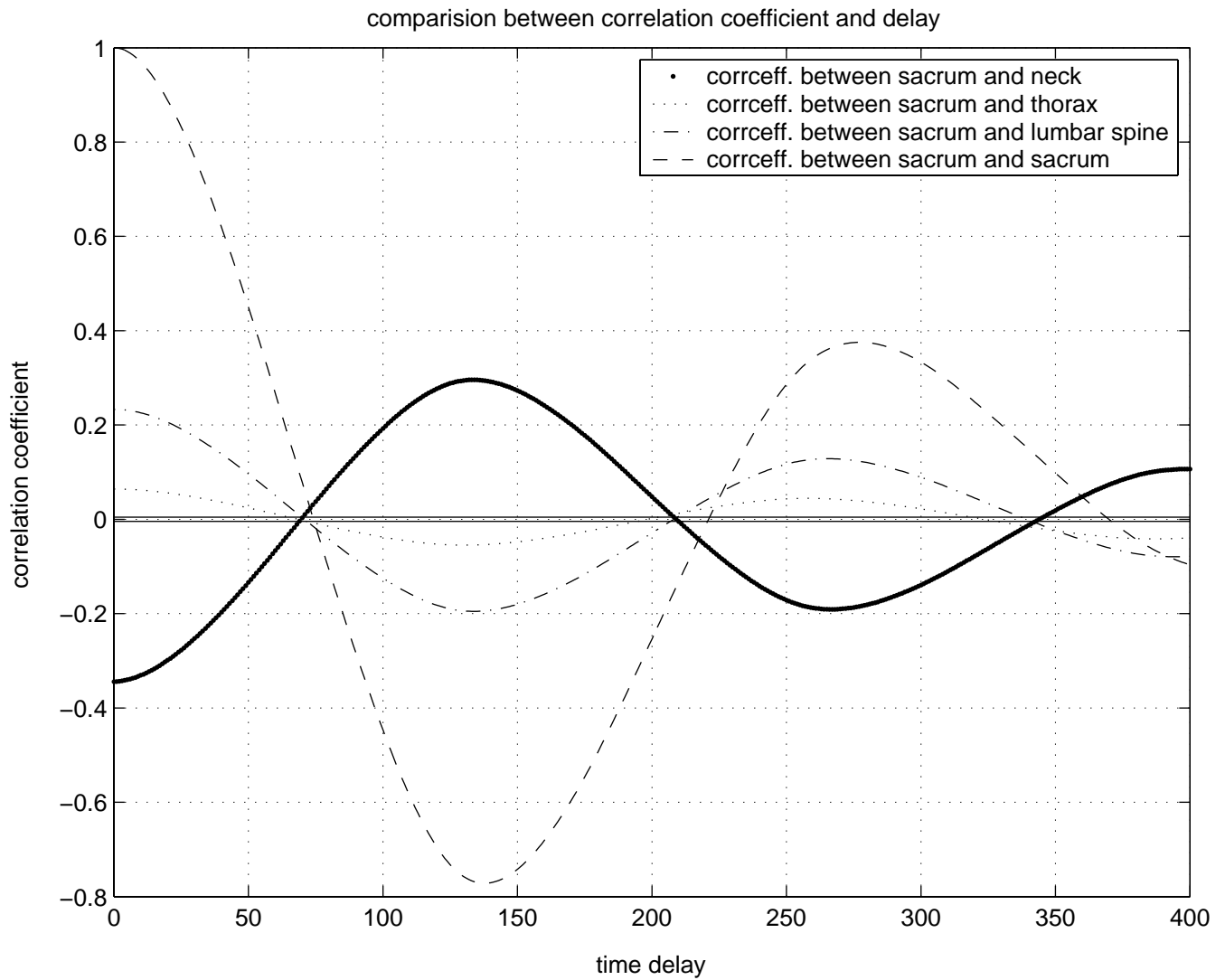


Figure 14: Correlation between subbands of sacrum and other signals for baseline subject BL04.

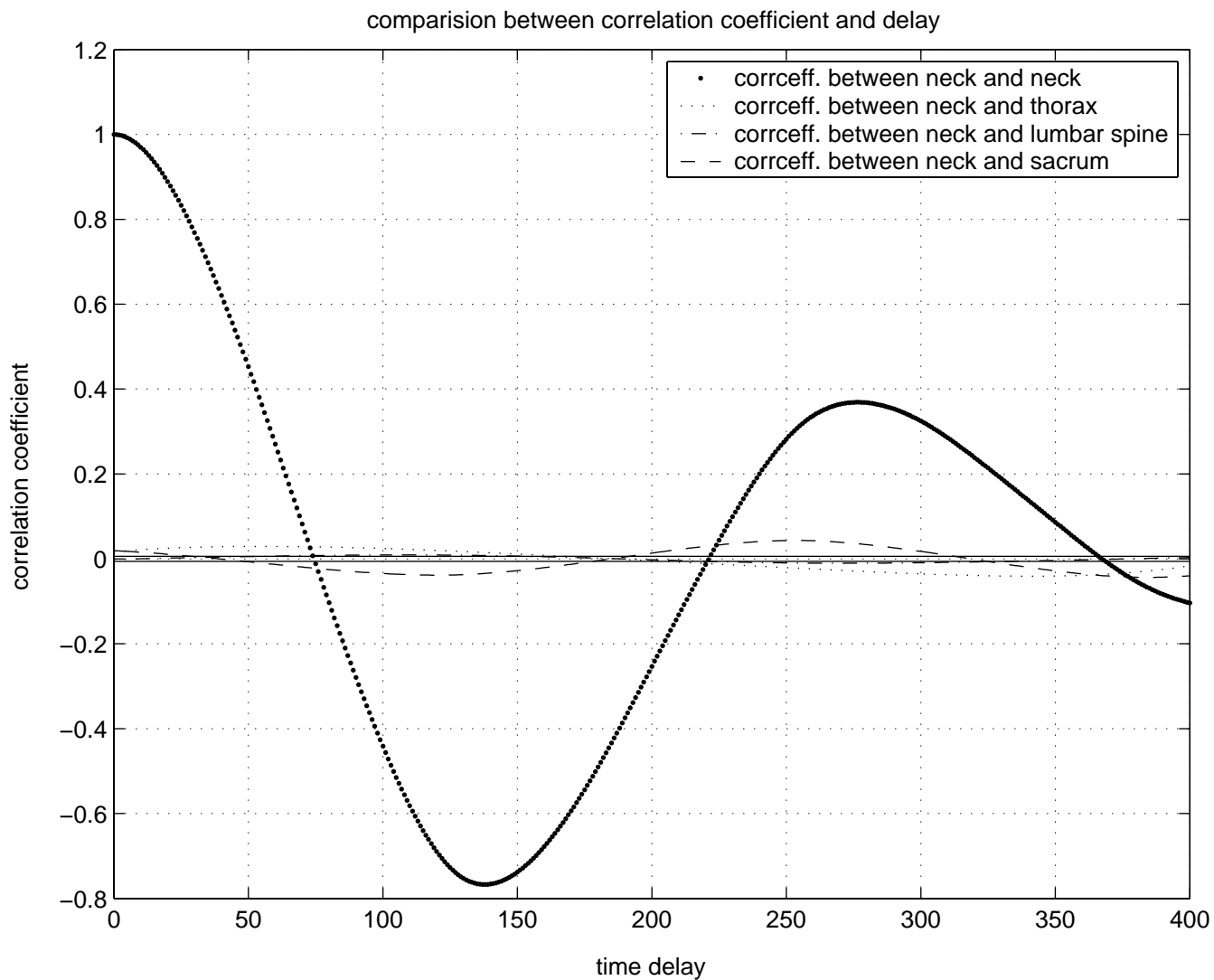


Figure 15: Correlation between subbands of neck and other signals for quadriplegic subject Q04.

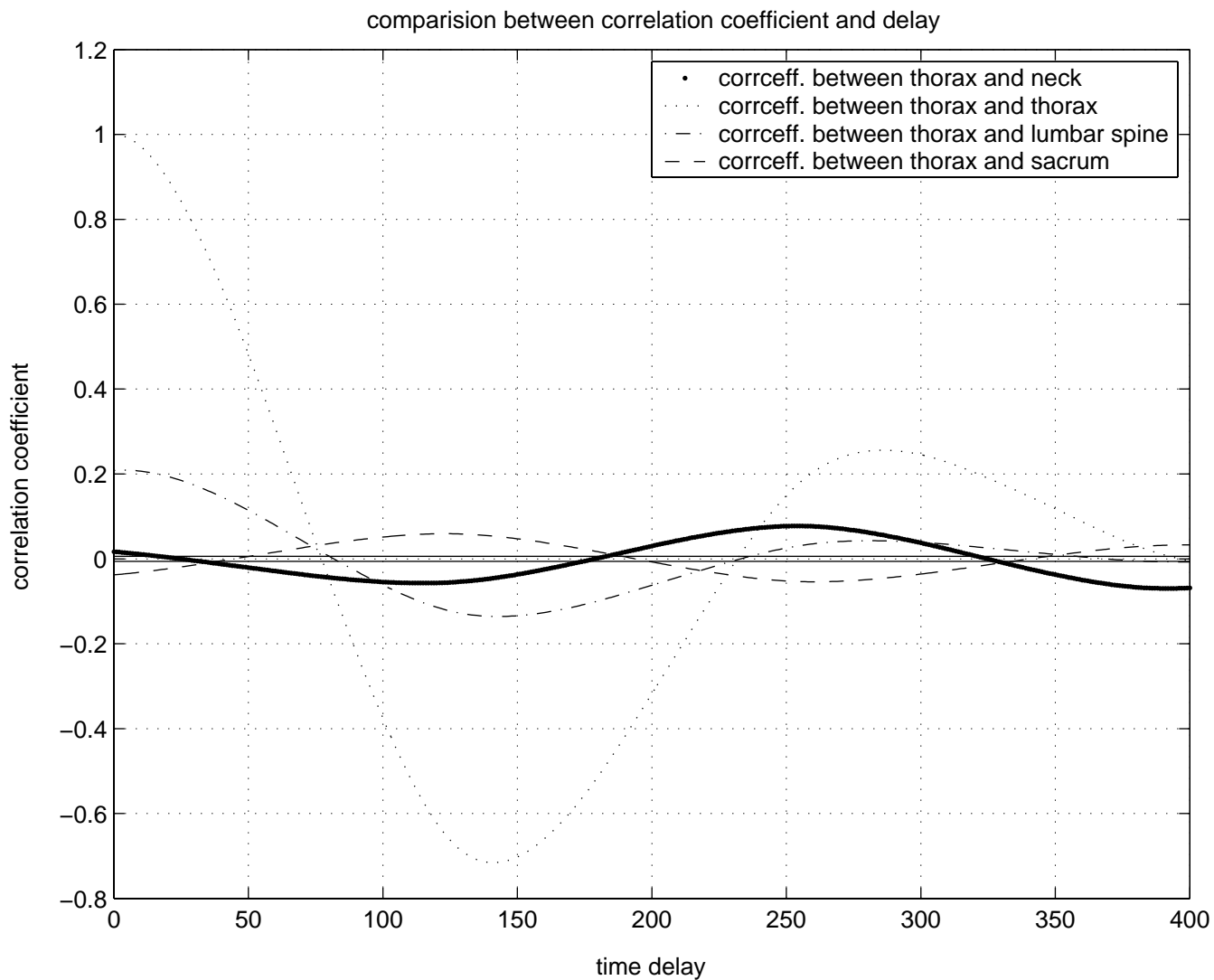


Figure 16: Correlation between subbands of thorax and other signals for quadriplegic subject Q04.

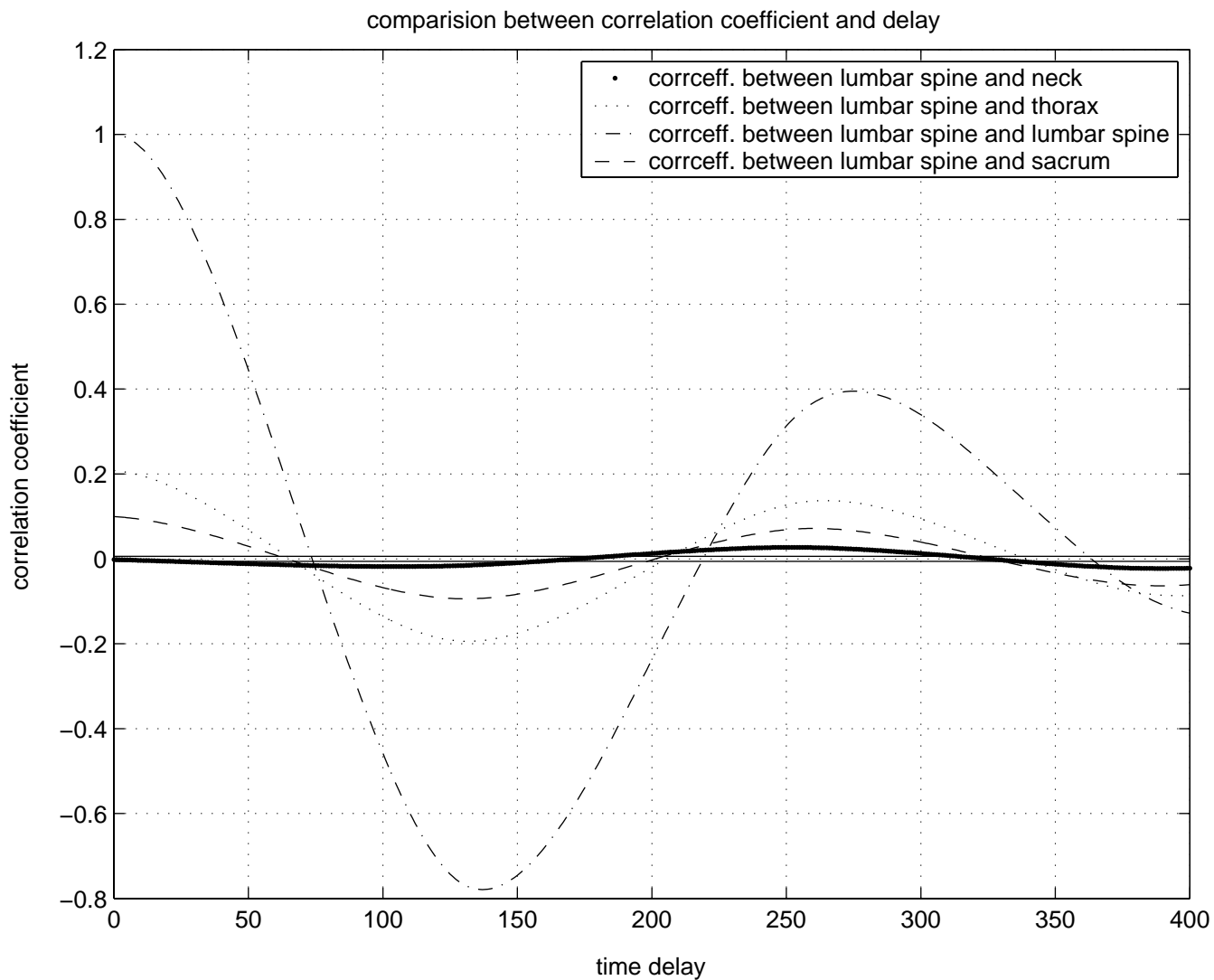


Figure 17: Correlation between subbands of lumbar spine and other signals for quadriplegic subject Q04.

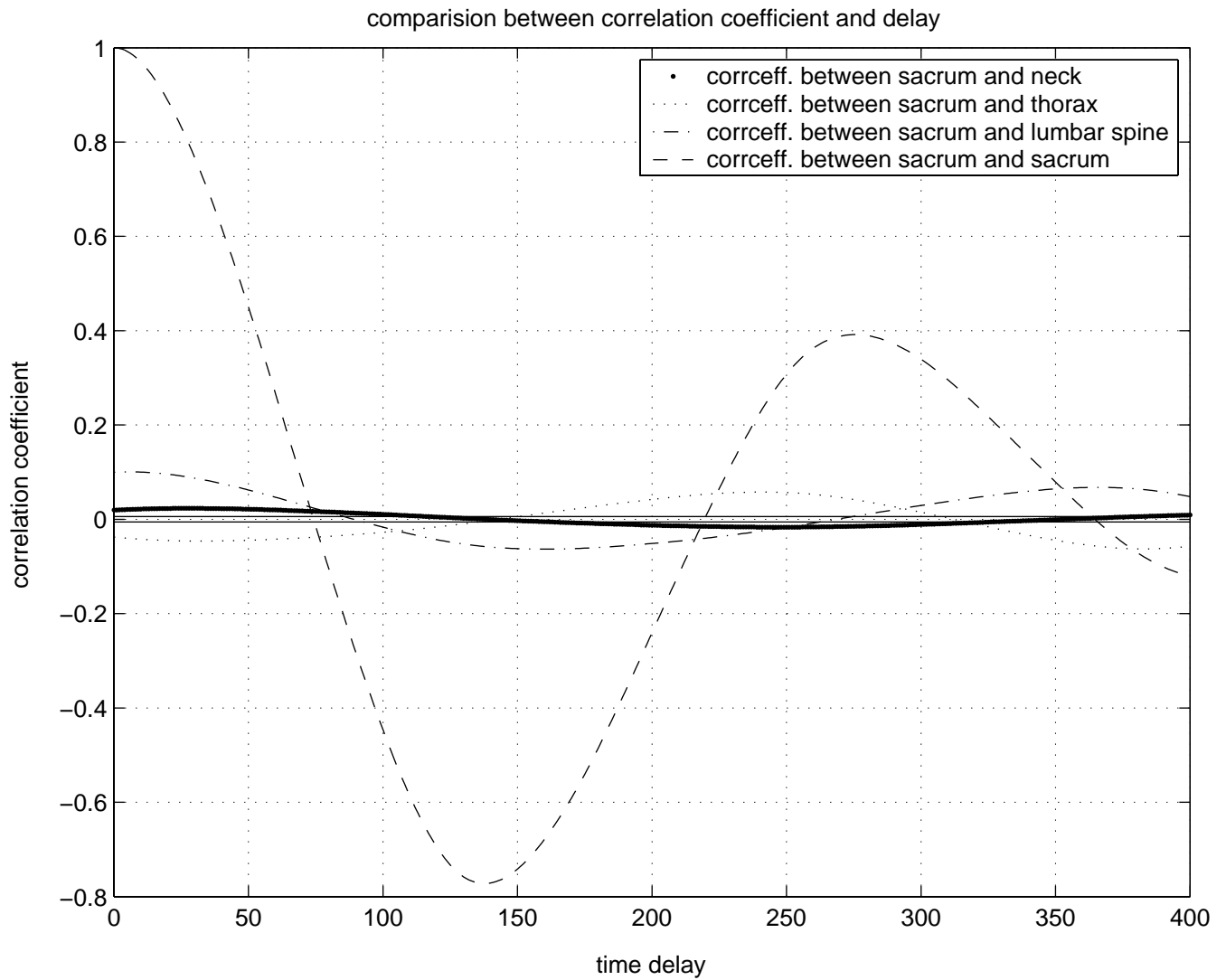


Figure 18: Correlation between subbands of sacrum and other signals for quadriplegic subject Q04.

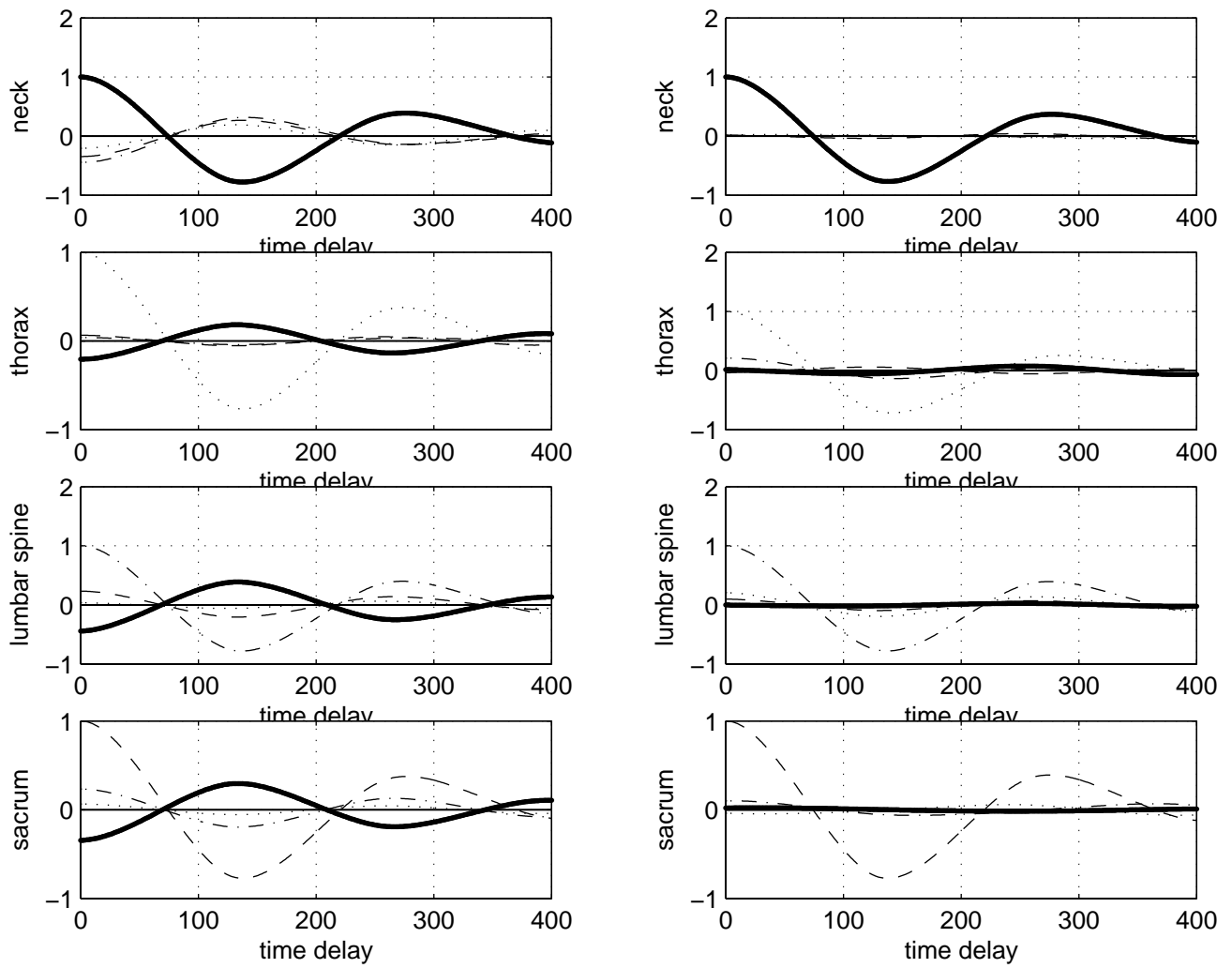


Figure 19: Comparison between correlation curves of baseline (left) and quadriplegic (right) subjects.

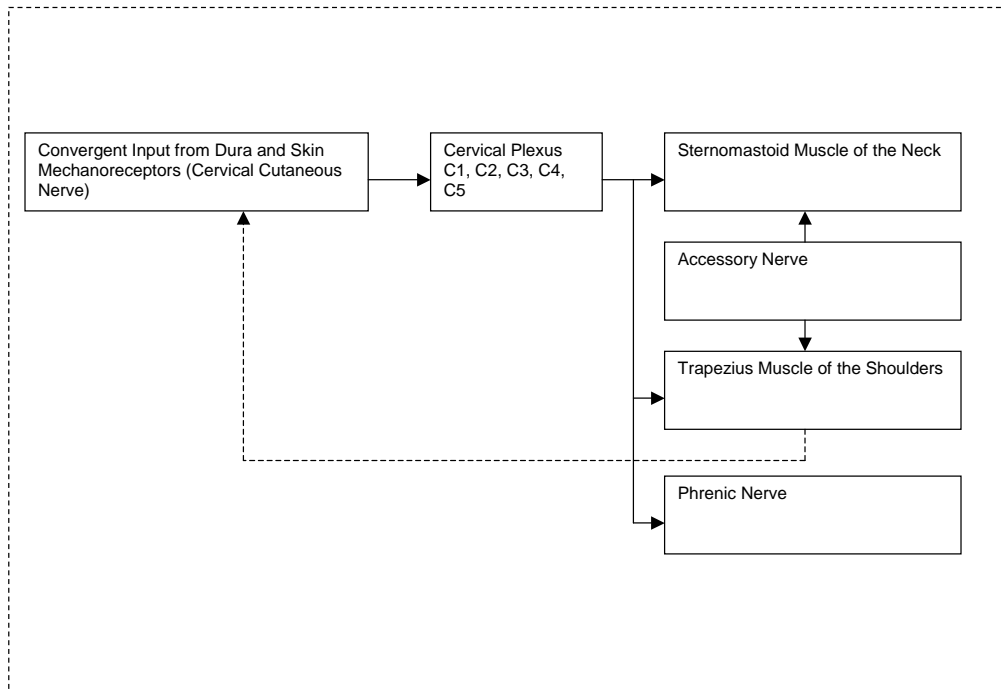


Figure 20: Sensory-motor instability loop at cervical level. The hard lines are established nervous pathways, while the dotted feedback line is the most likely motor-sensory path based on Alf Breig's model and our visual observations and sEMG analysis.

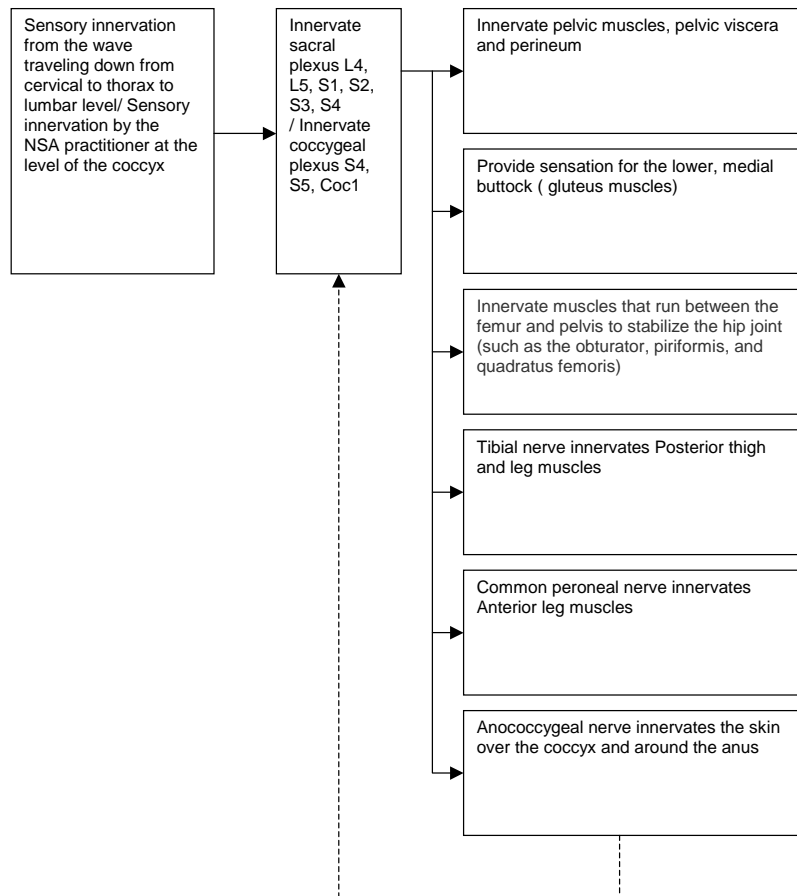


Figure 21: Sensory-motor instability loop at sacral level. The hard lines are established nervous pathways, while the dotted feedback line is the most likely motor-sensory path based on our visual observations and sEMG analysis.